Caenorhabditis elegans PIEZO Channel Coordinates Multiple Reproductive Tissues to Govern Ovulation

Running Title: PEZO-1 is Required for Ovulation

Xiaofei Bai[1], Jeff Bouffard[3], Avery Lord[2], Katherine Brugman[4], Paul W. Sternberg[4], Erin J. Cram[2], Andy Golden[1]*

[1]National Institute of Diabetes and Digestive and Kidney Diseases, National Institutes of Health, Bethesda, MD.

[2]Department of Biology, Northeastern University, Boston, MA.

[3]Department of Bioengineering, Northeastern University, Boston, MA.

[4]Division of Biology and Biological Engineering, California Institute of Technology, Pasadena, CA.

* Corresponding Author:

Andy Golden

Building 8, Room 323

8 Center Dr.

Bethesda, MD 20892

(301) 594 4367

E-mail: andyg@nih.gov

ORCIDs:

X.F.B. ORCID: 0000-0001-8179-8162, K.B. ORCID: 0000-0003-2625-2903, P.W.S. ORCID: 0000-0002-7699-0173, E.J.C. ORCID: 0000-0002-8129-1326, A.G. ORCHID: 0000-0002-8599-2031.

Abstract

PIEZO1 and PIEZO2 are newly identified mechano-sensitive ion channels that exhibit a preference for calcium in response to mechanical stimuli. In this study, we discovered the vital roles of *pezo-1*, the sole *PIEZO* ortholog in *C. elegans,* in regulating reproduction. A number of deletion alleles as well as a putative gain-of-function mutant of PEZO-1 caused a severe reduction in brood size. *In vivo* observations showed that oocytes undergo a variety of transit defects as they enter and exit the spermatheca during ovulation. Post ovulation oocytes were frequently damaged during spermathecal contraction. However, the calcium signaling was not dramatically changed in the *pezo-1* mutants during ovulation. Loss of PEZO-1 also revealed an inability of self-sperm to properly navigate back to the spermatheca after being pushed out of the spermatheca during ovulation. These findings suggest that PEZO-1 acts in different reproductive tissues to promote proper ovulation and fertilization in *C. elegans*.

Introduction

Mechanotransduction - the sensation and conversion of mechanical stimuli into biological signals - is essential for development. PIEZO1 and PIEZO2 are newly identified excitatory mechanosensitive proteins, which play important roles in a wide range of developmental and physiological processes in mammals (Alper, 2017; Coste et al., 2010; Coste et al., 2012; Murthy et al., 2017; Wu et al., 2017). PIEZO1 is a non-selective ion channel that forms homotrimeric complexes at the plasma membrane, however, PIEZO1 exhibits a preference for Ca^{2+} in response to mechanical stimuli (Coste et al., 2010; Gnanasambandam et al., 2015; Syeda et al., 2015). Recent studies have shown that the human and mouse PIEZO1 channels respond to different mechanical stimuli, including static pressure, shear stress and membrane stretch (Coste et al., 2010; Poole et al., 2014; Ranade et al., 2014). PIEZO1 also regulates vascular branching and endothelial cell alignment upon sensing frictional force (shear stress) (Li et al., 2015; Nonomura et al., 2018). Stem cells also use PIEZO1 to sense mechanical signals and initiate Ca^{2+} signaling to promote proliferation and differentiation (Del Marmol et al., 2018; He et al., 2018). PIEZO2 primarily functions as a key mechanotransducer for light touch, proprioception and breathing (Nonomura et al., 2017; Woo et al., 2015; Woo et al., 2014). Mutations in both human *PIEZO1* and *PIEZO2* have been identified among the patients suffering from channelopathy diseases, such as Dehydrated Hereditary Stomatocytosis (DHSt), Generalized Lymphatic Dysplasia (GLD), and Distal Arthrogryposis type 5 (DA5), in which osmoregulation is disturbed (Albuisson et al., 2013; Andolfo et al., 2013; Bae et al., 2013; Coste et al., 2013; Li et al., 2018; Lukacs et al., 2015; McMillin et al., 2014;

Zarychanski et al., 2012). Loss-of-function mutations in the *PIEZO1* gene cause autosomal recessive congenital lymphatic dysplasia while gain-of-function mutations lead to autosomal dominant stomatocytosis (Alper, 2017). However, the cellular and molecular mechanisms of PIEZO dysfunction in these diseases are not well understood.

Caenorhabditis elegans is an attractive model system to study mechanotransduction *in vivo. C. elegans* contains multiple tubular tissues, including the reproductive system, which experience mechanical stimulation (Cram, 2014, 2015; Voglis and Tavernarakis, 2005). The *C. elegans* reproductive system consists of two U-shaped gonad arms, each ending with a spermatheca and joined in the center by a shared uterus. *C. elegans* hermaphrodites produce sperm during the L4 larval stage and then shift to produce oocytes during the adult stage. About 150 sperm are stored in each spermatheca while the oocytes form in the oviduct in each gonad arm. The oocyte adjacent to the spermatheca undergoes oocyte maturation ~25 minutes before being ovulated into the spermatheca (Greenstein, 2005). Oocyte maturation is triggered by sperm-derived polypeptides known as major sperm proteins (MSPs), which activate the oocyte mitogen-activated protein kinase (MPK-1) (Miller, 2001; Yang et al., 2010). Once the oocyte matures, five pairs of contractile myoepithelial cells that make up the somatic gonad and encase the germline, named sheath cells, push the matured oocyte into the spermatheca for fertilization. The spermatheca is an accordion-like multicellular tube, consisting of two spermathecal valves, the distal valve closest to the oviduct and spermathecal-uterine (sp-ut) valve, and a bag-like chamber between the two valves (Kimble and Hirsh, 1979; McCarter et al., 1999). These two spermathecal valves are

spatiotemporally coordinated to allow oocyte entry during ovulation and exit after fertilization, through acto-myosin contractions (Kelley and Cram, 2019). Ovulation is triggered by signaling between oocytes, sheath cells, and sperm through increasing cytosolic inositol 1,4,5-trisphosphate (IP_3) and Ca^{2+} concentrations (Bui and Sternberg, 2002; Clandinin et al., 1998; Han et al., 2010). The ovulated oocyte spends 3-5 minutes in the dilated spermatheca with both valves closed to allow the oocyte and sperm to complete fertilization and to initiate eggshell formation (Johnston et al., 2010). The constriction of the spermathecal bag cells and the opening of the spermathecal-uterine valve cells expel the fertilized egg into the uterus. Meanwhile, the sperm that are swept out of the spermatheca during oocyte exit crawl back to the constricted spermatheca. The navigation of the sperm back to the spermatheca is regulated by the chemoattractant prostaglandin that is secreted by the oocytes and sheath cells (Kubagawa et al., 2006). Despite the probable role of mechanical stimuli during this whole process, such as stretch of oocyte entry or the contraction of the spermatheca, the mechanisms underlying the mechanosensitive channels in ovulation and fertilization remain largely unknown.

In this study, we hypothesized that a mechanosensitive protein like PEZO-1, the sole PIEZO-like protein in *C. elegans,* would be involved in processes that include such cellular movements as those observed in ovulation, where oocytes must transit into and out of the spermatheca. Multiple deletion mutations, as well as a putative gain-of-function mutation, caused severe reproductive deficiencies, such as reduced brood sizes and defects in ovulation and sperm navigation. Somewhat surprisingly, normal

calcium release was observed in the spermatheca during early ovulations of *pezo-1* mutants compared with wild type. Sperm that were readily washed out of the spermatheca during ovulation failed to migrate back to the spermatheca, thus depleting the spermatheca of sperm early in the reproductive lifecycle. Supplementing male sperm via mating significantly repopulated the spermatheca with cross-sperm and rescued the extremely low ovulation rate and reduced brood size in *pezo-1* mutants. Using an auxin-inducible degradation (AID) system, we depleted PEZO-1 in somatic tissues and the germline. Reduced brood sizes were observed in each tissue-specific degradation strain, suggesting multiple inputs of PEZO-1 from many tissues in regulating reproduction. Thus, our analysis of numerous *pezo-1* mutants suggests a complex role in a number of tissues required for reproduction.

Results

PEZO-1 is expressed in multiple tissues throughout development

The *C. elegans* genome encodes a single *PIEZO* ortholog, *pezo-1*, of which there are 14 mRNA isoforms due to differential splicing and transcriptional start sites (Fig.1-figure supplement 1A) (Harris et al., 2019); these 14 isoforms code for 12 different PEZO-1 proteins. All isoforms share a common C-terminus. To accurately visualize the expression pattern of *pezo-1 in vivo*, we directly knocked-in different fluorescent reporter genes into both the N-terminus and C-terminus of the *pezo-1* endogenous locus using CRISPR/Cas9. The C-terminal knock-in reporters should tag all *pezo-1* isoforms, while the N-terminal knock-in reporters should only tag the eight longest *pezo-1* isoforms (Fig.1A, Fig.1-figure supplement 1A). Both GFP and mScarlet were used as reporters to generate N- and C-terminal fusions proteins. GFP::PEZO-1, mScarlet::PEZO-1, and PEZO-1::mScarlet were widely expressed from embryonic stages through adulthood (Fig. 1B-E, G-J, Fig.1-figure supplement 1B-G). The genome-edited animals behaved normally, suggesting no functional disruption of tagging PEZO-1 with these fluorescent reporter genes. Notably, PEZO-1 is strongly expressed in several tubular tissues, including the pharyngeal-intestinal and spermathecal-uterine valves, which is consistent with our hypothesis that *pezo-1* may be responsible for mechanoperception in these tissues (Fig. 1B, Fig.1-figure supplement 1B, C). Under higher magnification, we observed PEZO-1 on the plasma membranes of oocytes and embryonic cells during a variety of embryonic stages, suggesting PEZO-1 is a transmembrane protein (Fig. 1C-E). PEZO-1 is expressed in multiple reproductive tissues, including the germline, somatic oviduct, and spermatheca (Fig. 1F-J). Higher

magnification imaging of the spermatheca revealed expression of PEZO-1 on sperm membranes as well (Fig. 1J). Consistent with the hypothesis that reproductive tissues are regulated by mechanosensitive stimuli in *C. elegans*, expression of PEZO-1 likely functions to sense physical strain or contractility during ovulation and fertilization. Live imaging and detailed analysis of PEZO-1 expression patterns during reproduction revealed that GFP::PEZO-1 is expressed in sheath cells, sperm, both spermathecal valves and the spermathecal bag cells (Fig. 1K-O, Video 1). The fluorescent signal of GFP::PEZO-1 is observed in both spermathecal valves, suggesting that PEZO-1 may function to sense the mechanical stimuli at the valves during ovulation (Fig. 1K, M, N, Video 1). As the fertilized oocyte is pushed into the uterus, GFP::PEZO-1 labeled sperm crawl back into the constricting spermatheca after each ovulation (Fig. 1O, Video 1). Collectively, these data indicate that PEZO-1 is expressed in the somatic gonadal cells and germline cells.

Deletion of *pezo-1* causes a decrease in brood size

To investigate the function of *pezo-1*, the phenotypes of *pezo-1* knockout (*pezo-1*^{KO}) animals were analyzed. Three candidate null alleles were generated by CRISPR/Cas9 genome editing; one allele was a deletion of exons 1-13 (*pezo-1 NΔ*), a second bearing a deletion of the last seven exons, 27-33 (*pezo-1 CΔ*) (Fig.2-figure supplement 1A, B), and a third bearing a full-length deletion of the entire *pezo-1* coding sequence (*pezo-1* full deletion). Two other alleles were generated by CRISPR/Cas9: *pezo-1(sy1398)*, which has a deletion of an exon unique to the two shortest isoforms, i and j, and a putative null allele, *pezo-1(sy1199),* which has a “STOP-IN” mutation in

exon 27 that should interfere with translation of the C-termini of all isoforms (Fig.2-figure supplement 1B). Although GFP::PEZO-1 and PEZO-1::mScarlet expressed widely in adult worms, we did not observe obvious morphological phenotypes from homozygous *pezo-1*^{KO} mutants compared to control animals. However, in all tested *pezo-1* mutants, the number of F1 progeny was significantly reduced compared with wild type (Fig. 2A, Fig.2-figure supplement 1C). The decrease in brood size was enhanced as animals aged (36-60 hours post mid-L4, Fig.2-figure supplement 1C) or when grown at a higher temperature (25°C, Fig.2-figure supplement 1D). In addition, about 5-25% of F1 embryos failed to hatch from *pezo-1 CΔ* homozygous mutants (Fig. 2B). To mimic a gain-of-function phenotype in *pezo-1*, we fed wildtype animals with Yoda1, a PIEZO1 specific chemical agonist, which keeps the channel open (Syeda et al., 2015). Reduced brood sizes were observed when wildtype animals were exposed to 20 μM Yoda1 (Fig. 2C). This phenotype did not worsen when *pezo-1*^{KO} animals were also treated with Yoda (Fig. 2C). These data suggest that either deletion or overactivation of PEZO-1 is sufficient to disrupt brood size.

Severe ovulation defects were observed in the *pezo-1* mutants

Using differential interference contrast (DIC) and confocal microscopy, we analyzed the defects associated with the observed reduction in brood size. While embryos fill the uterus in wildtype mothers (Fig. 2D), a mass of ooplasm in the uteri of both *pezo-1*^{KO} and STOP-IN mutants was observed (Fig. 2E, Fig.2-figure supplement 1E). Occasionally, a few fertilized embryos were observed inside this mass of ooplasm (data not shown). *pezo-1 CΔ* and STOP-IN mutants displayed the most severe defects,

where 100% of animals had a uterus filled with ooplasm at 60 hours post L4 (Fig. 2F, Fig.2-figure supplement 1E). Staining with DAPI in *pezo-1*^{KO} uteri revealed chromosome structures indicative of diakinesis-staged oocytes (Fig. 2H). Sperm chromatin was not clearly observed so we cannot state for certain that these crushed oocytes were not fertilized. In contrast, only mitotic chromatin of variably-aged embryos were detected in control animals (Fig. 2G). Consistent with this observation, only unfertilized oocytes and newly-fertilized embryos without intact eggshells stained with the lipophilic dye, BODIPY, in wildtype animals (Fig. 2I). BODIPY staining revealed widespread penetration of the entire ooplasmic mass in the uteri of *pezo-1 CΔ* animals (Fig. 2J). These data suggest that some oocytes are not fertilized upon transit through the spermatheca and that these unfertilized oocytes may be crushed when they pass through the spermathecal valves. Though these crushed oocyte phenotypes are reminiscent of those observed in animals depleted of some eggshell components (Johnston et al., 2010), there are notable differences. The *pezo-1* mutant oocytes are not fertilized and do not make an eggshell. The lack of fertilization or eggshell synthesis is not likely to be responsible for the crushed oocyte phenotype as the oocytes in *spe* mutants survive spermatheca transit and often get laid after passing through the uterus. A more detailed characterization of the ovulation defects is described below.

In addition to these apparent crushed oocytes, reduced numbers of sperm resident in the spermatheca were observed in Day 1 *pezo-1* adults (0-24 hours post mid-L4) and even fewer were observed in the spermathecae in Day 2-3 adults (24-48 hours post mid-L4) compared with wild type (Fig. 2K-M). Normal numbers of sperm were present in these mutant hermaphrodites prior to the first ovulation, suggesting that

212 the ability of the sperm to return to the spermatheca after each ovulation was disrupted
213 (Fig. 2M). Sperm loss could also contribute to the low brood sizes observed in our *pezo-*
214 1 mutants.

215 Ovulation rates were significantly reduced in *pezo-1 CΔ* Day 2 (post mid-L4 48
216 hours) animals (Fig. 2N), which is consistent with the reduced brood sizes that worsen
217 in Day 2 animals. Since sperm presence in the spermatheca is known to stimulate
218 ovulation (McCarter et al., 1999; Miller, 2001), the reduction in sperm number could be
219 responsible for this reduction in ovulation rate. Overall, the reduced brood size in *pezo-1*
220 mutants is likely due to a combination of defects in multiple tissues, resulting in
221 defective ovulations, crushed oocytes, and defects in the ability of sperm to navigate
222 back into the spermatheca after each ovulation.

223 To carefully characterize the transit of oocytes through the spermatheca, we
224 performed live imaging to record the ovulation and fertilization process in both wildtype
225 and *pezo-1*^{KO} animals (Fig. 3 A-E', Videos 2, 3). The imaging began with the mature
226 oocyte entering the spermatheca, labeled by the apical junction marker DLG-1::GFP
227 (Fig. 3A, B). In wildtype animals, the contracting sheath cells push the oocyte into the
228 spermatheca, and simultaneously pull the open spermatheca over the oocyte (Videos 2,
229 3). Once the oocyte enters the spermatheca, both spermatheca valves remain closed
230 during fertilization (Fig. 3C). Opening of the sp-ut valve allows the fertilized oocyte to be
231 expelled into the uterus (Fig. 3D, E). In *pezo*-1 mutants, of the oocytes that did
232 successfully enter the spermatheca, many were crushed when they exited through the
233 sp-ut valve (Fig. 3A'-E', Videos 2, 3). We observed that the sp-ut valve, labeled by DLG-
234 1::GFP, did not completely open when the oocyte attempted to exit the spermatheca,

which may lead to crushing the oocyte (Fig. 3C'-E', Video 3). The ooplasm from the crushed oocytes accumulated in the uterus (Fig. 3E', Video 3) as a large ooplasmic mass (as shown in Fig. 2E). During our analysis of the *pezo-1* mutants, we frequently observed that oocytes partially entered the spermatheca but were then pinched off and broken into two pieces, one of which remained trapped in the oviduct (proximal gonad; Fig. 3F-I, Video 4). Moreover, some oocytes failed to enter the spermatheca and slid back into the oviduct (Fig. 3J-M, Video 5). The defective ovulation is likely due to incomplete constriction of the sheath cells. Overall, disrupted ovulation and oocyte transit defects were observed in *pezo-1* mutants, consistent with the decreased brood size observed in all of our *pezo-1* mutants.

PEZO-1 mutants are affected upon depletion of cytosolic Ca^{2+} regulators.

Given that PEZO-1 is the ortholog of mammalian mechanosensitive calcium channels and that Ca^{2+} signaling is a major regulator of *C. elegans* spermathecal contractility, we tested whether there was suppression or enhancement when *pezo-1* mutants were combined with the depletion of several important cytosolic Ca^{2+} regulators. To manipulate potential calcium signaling, an ER Ca^{2+} release channel, ITR-1, and an inositol-1,4,5-triphosphate (IP_3) kinase, LFE-2, were depleted by RNAi in both wildtype and *pezo-1* mutants. IP_3 binding to ITR-1 releases Ca^{2+} from the ER, which activates myosin for spermathecal contractility (Bouffard et al., 2019; Clandinin et al., 1998; Kovacevic et al., 2013). Therefore, we hypothesized that combining *pezo-1* mutants with *itr-1* RNAi would greatly enhance the reduction in brood size if they were both critical to ovulation and fertilization. We carefully calibrated *itr-1* RNAi treatment

and determined that feeding L4 animals for 36-60 hours produced optimal intermediate conditions that caused minimal developmental defects and normal brood sizes in wildtype animals. Consistent with our hypothesis, feeding *itr-1* RNAi resulted in even smaller broods than observed in *pezo-1* mutants alone (Fig. 4A). In contrast, feeding *lfe-2* RNAi, which should elevate cytosolic Ca^{2+}, partially rescued the reduced brood size (Fig. 4B). Therefore, *pezo-1*^{KO} mutants were further compromised with *itr-1*(RNAi), yet partially rescued when combined with *lfe-2* (RNAi). Similarly, depletion of the plasma membrane Ca^{2+} channel *orai-1*, which is activated to replenish the extracellular Ca^{2+} to the cytosol (Lorin-Nebel et al., 2007), led to nearly zero brood size in *pezo-1 CΔ* mutant but only a 40% reduction in brood size in wild type (Fig. 4C). Furthermore, disruption of ER Ca^{2+} stores with sarcoplasmic/ER Ca^{2+} ATPase (SERCA) *sca-1*(RNAi) (Yan et al., 2006) also caused an extremely low brood size in *pezo-1 CΔ* (Fig. 4C) while *sca-1*(RNAi) slightly increased the brood size in wild type (Fig. 4C). Therefore, these observations are consistent with the hypothesis that *pezo-1* may function in cytosolic and ER Ca^{2+} homeostasis, which is crucial for proper spermathecal contractility and dilation.

***pezo-1* mutants show normal calcium signaling in spermatheca cells during ovulation.**

Due to PIEZO channels' permeability to Ca^{2+} and the importance of calcium signaling in regulating spermathecal contractility, we tested whether deletion of *pezo-1* disrupted cytosolic Ca^{2+} homeostasis. We imaged oocyte passage through the spermathecae of both wild type and *pezo-1* mutants expressing the Ca^{2+} indicator

GCaMP3, which was driven by a spermatheca-specific *fln-1* promoter (Bouffard et al., 2019; Kovacevic et al., 2013). Co-localization of the GCaMP3 transgene with mScarlet::PEZO-1 in the spermatheca suggested that this transgene would be useful for the analysis of *pezo-1* function in spermathecal calcium signaling (Fig 5A-E, Video 6). To determine whether calcium signaling was altered in our *pezo-1* mutants, a set of high-speed GCaMP imaging data from different animals was generated and the average pixel intensity of each frame was quantified (Fig 5F-J', Fig.5-figure supplement 1A-D, Video 6). We defined the initial time frame as the time just before the oocyte entered the spermatheca. In wildtype animals, the fluorescent intensity of GCaMP3 at the sp-ut valve immediately increased when the oocyte entered the spermatheca (Fig 5A, F and F', Videos 6, 7). During fertilization, an increase in intensity of GCaMP3 was frequently observed in the bag cells and sp-ut valve until the oocyte exited the spermatheca (Fig 5B-D, G-I and G'-I', Videos 6, 7). GCaMP3 signal decreased to basal intensity after the fertilized oocyte was expelled into the uterus (Fig. 5E, J and J', Videos 6, 7). To statistically quantify and analyze the oocyte transit, we defined a series of parameters, including the dwell time and two calcium signaling metrics from the GCaMP3 time series (Bouffard et al., 2019). A spermathecal tissue function metric, dwell time, is defined as the time from spermathecal distal valve closure to sp-ut valve opening, which represents the duration of time that the oocyte resides in the enclosed spermatheca. The calcium signaling metric, fraction over half max, is defined as the duration of the dwell time over the GCaMP3 half-maximal value divided by the total dwell time. The fraction over half max allows us to capture the relative level of calcium throughout the time the embryo passes through the spermatheca. Rising time indicates

the time from the opening of the distal valve to the first time point at which the GCaMP fluorescent intensity reaches half maximum (Bouffard et al., 2019). In *pezo-1 CΔ* mutants, longer transit times of the oocyte through the spermatheca resulted in elongated dwell times (Fig. 5K, Video 7), suggesting that deletion of *pezo-1* resulted in disrupted tissue function. Surprisingly, GCaMP3 fluorescence in *pezo-1* was not significantly different than wildtype (Fig. 5L, M, Video 7; see methods). GCaMP3 time series (Fig.5-figure supplement 1A, B, Video 7), heat maps (Fig.5-figure supplement 1C), and kymograms (Fig.5-figure supplement 1D, E) also displayed normal Ca^{2+} levels during oocyte passage through the spermatheca in *pezo-1* mutants. It should be noted that we only imaged the GCaMP3 reporter during the very first three ovulations in young adult animals to avoid Ca^{2+} signaling interference from a distorted gonad morphology and mechanical pressure from a gravid uterus. Furthermore, it is difficult to monitor older *pezo-1* hermaphrodites as they do not ovulate on microscope slides. Since only mild defects were observed in the *pezo-1* mutants during these early ovulations and oocyte transit defects increased in severity over time (Fig. 2F), our data does not exclude the possibility that Ca^{2+} signaling may be more severely disrupted as the animal goes through more ovulation cycles. Alternatively, the live imaging assay may not be sensitive enough to detect subtle variations in calcium signaling.

Sperm from matings rescues low brood size phenotype in *pezo-1* mutants

In *C. elegans*, successful ovulation and fertilization requires signal coordination between sperm, oocytes, and sheath cells (Han et al., 2010). Given that PEZO-1 is expressed in these tissues, it is plausible that oocyte transit defects and reduced brood

sizes are due to impaired inter-tissue signaling, which may be mediated by PEZO-1. To investigate how this may occur, bidirectional signaling between sperm and oocytes was first tested. To test for the ability of sperm to fertilize oocytes, both wildtype and *pezo-1* mutant males were mated with *fem-1(hc17)* hermaphrodites, which do not produce any sperm or self-progeny (Doniach and Hodgkin, 1984) and are essentially females. The *fem-1(hc17)* animals produced cross-progeny after mating with *pezo-1* mutant males, indicating *pezo-1* mutant males are fertile and that their sperm can crawl through the uterus to the spermatheca upon mating (Fig. 6A). Since *pezo-1* mutant hermaphrodites do not produce any self-progeny after Day 3 (60 hours post mid-L4) (Fig. 6B), we tested whether mating with either wildtype or mutant males would result in any cross progeny in the aged *pezo-1* mutants. *pezo-1* mutant hermaphrodites resumed ovulation and fertilization upon mating once the male's sperm (from either wildtype or *pezo-1* males) reached the spermatheca (Fig. 6B-D). To test whether sperm signaling was defective in inducing ovulation in *pezo-1* mutants, we mated both *spe-9(hc52ts)* and control *him-8(e1489)* males with both wildtype and *pezo-1* mutant hermaphrodites. *spe-9(hc52ts)* male sperm can physically contact the oocytes but fail to fertilize, however, the sperm signaling is apparently normal and triggers ovulation (Singson et al., 1998). Interestingly, the low ovulation rate in older *pezo-1 CΔ* animals was significantly rescued by *spe-9(hc52ts)* sperm (Fig. 6E), although the ovulated oocytes were not fertilized. An additional experiment was performed to test the ability of the sheath to respond to the sperm signal which triggers ovulation. Even though our data in Fig. 6E suggests that just the presence of sperm can trigger ovulation, we went on to show that purified MSP-fluorescein can also trigger ovulation in older *pezo-1 C*Δ hermaphrodites

that are depleted of sperm and are no longer ovulating (Fig. 6F-H). Overall, these data suggest that the absence of self-sperm contributes to a profound reduction of oocyte maturation, ovulation rate, and self-fertility in the aged *pezo-1* mutants.

Sperm guidance and navigation is disrupted in *pezo-1* mutants

In wildtype hermaphrodites, the sperm are constantly being pushed out of the spermatheca each time the sp-ut valve opens to expel the fertilized oocyte into the uterus. These sperm, however, are fully capable of crawling back to the spermatheca to induce high levels of oocyte maturation and ovulation (Miller, 2001; Miller et al., 2003). This is a very efficient mechanism such that almost every self-sperm in a hermaphrodite is used to fertilize an oocyte. It is sperm number that defines brood size; oocytes are in excess. Oocytes secrete F-series prostaglandins derived from polyunsaturated fatty acids (PUFAs) to guide sperm to the spermatheca (Han et al., 2010; Kubagawa et al., 2006). To test whether *pezo-1* hermaphrodites fail to attract the sperm back to the spermatheca, male sperm navigational performance was assessed *in vivo* by staining males with a vital fluorescent dye, MitoTracker CMXRos, which efficiently stains sperm in live animals (Whitten and Miller, 2007). Both wildtype and *pezo-1 CΔ* stained males were mated to non-labeled wildtype hermaphrodites for 30 minutes. The sperm distribution was assessed and quantified by dividing the uterus into three zones (Fig. 7A) and counting the number of fluorescent sperm in each zone (McKnight et al., 2014) one hour after males were removed from the mating plates. In wildtype hermaphrodites, most fluorescent sperm from both wildtype and *pezo-1 CΔ* males navigated through the uterus and accumulated in the spermatheca (Fig. 7B, C, F, G). However, fewer

fluorescent male sperm reached the spermatheca in Day 3 adult *pezo-1 CΔ* hermaphrodites and most sperm remained throughout zone1 and zone 2, the zones furthest from the spermatheca (Fig. 7D, E, H, I). This was observed for both wildtype and *pezo-1* mutant male sperm in mating with *pezo-1 CΔ* hermaphrodites (Fig. 7J). These observations suggest that in the wildtype hermaphrodite reproductive tracts, *pezo-1* mutant male sperm are motile and display normal navigational behavior. However, in *pezo-1* mutant hermaphrodite reproductive tracts, both wildtype and *pezo*-1 mutant sperm were compromised in their navigational behavior over the time frame of this experiment. Though it remains possible that the ooplasmic masses that accumulate in the uterus of *pezo-1* mutant hermaphrodites could physically interfere with the migration of wildtype and *pezo-1* mutant sperm back to the spermatheca, our labeled sperm experiments with female *pezo-1* mutants (see below) suggest that this is not a likely explanation.

To test whether the defective ovulation and sperm attraction were just self-sperm problems, we generated the same *pezo-1 CΔ* (used throughout this study) in temperature-sensitive *fem-1(hc17ts)* females. In *pezo-1 CΔ* female mutants, the number of F1 progeny was significantly reduced compared with control *fem-1(hc17ts)* at the permissive temperature of 15°C, which allows for the production of self-sperm (Fig.6-figure supplement 1A). We then mated these Day 2 (36 hours post mid-L4) females with both wildtype and mutant males and scored for cross progeny at the non-permissive temperature of 25°C. The male sperm were labeled by MitoTracker CMXRos before mating. We carefully quantified the number of male sperm in the reproductive tract of the *pezo-1 C*Δ females after mating for 30 minutes (Fig.6-figure supplement 1B). All

tested female animals sired crossed progeny but at greatly reduced levels in *pezo-1 CΔ* females (Fig.6-figure supplement 1C, D). This suggests that the attractive signal from the oocytes or sheath cells are defective in their ability to attract male sperm to the spermatheca. Thus, the defect in the ability to attract sperm to the spermatheca is not just a self-sperm problem; cross sperm from males also fail to migrate to the spermatheca.

The data shown in Fig. 6A and B suggests that mutant sperm, when mated with WT hermaphrodites or *fem-1* females, can migrate to the spermatheca and fertilize a large number of oocytes. However, when mated into the *pezo-1 C*Δ hermaphrodites, they do sire cross progeny but at greatly reduced levels compared to wildtype male sperm (Fig. 6B, right side). This result supports the conclusion that an attractive signal from the oocytes or sheath cells is missing or reduced in *pezo-1* hermaphrodites. Thus, we believe that there is not a problem with the ability of sperm to crawl and fertilize oocytes.

Tissue-specific degradation of PEZO-1 reveals multiple roles of PEZO-1 in both somatic tissues and germline cells

Our study aims to reveal the role of PEZO-1 in regulating reproduction and coordinating inter-tissue signaling. To dissect PEZO-1 function in distinct tissues, we utilized an auxin-inducible degradation system (AID) to degrade PEZO-1 in the soma and the germ line (Zhang et al., 2015). We knocked-in the degron coding sequence at the *pezo-1* C-terminus using CRISPR/Cas9 so that all isoforms would be targeted (Fig. 8A). To activate the AID system, this line was then crossed with the strains expressing

the degron interactor transgene *tir-1::mRuby* driven by the following promoters: $P_{eft\text{-}3}$, $P_{pie\text{-}1}$ and $P_{sun\text{-}1}$ (Zhang et al., 2015). $P_{eft\text{-}3}$*::tir-1::mRuby* was expressed in most or all somatic tissues, including the spermatheca and the sheath cells (Fig. 8B) while $P_{pie\text{-}1}$*::tir-1::mRuby* and $P_{sun\text{-}1}$*::tir -1::mRuby* were expressed in the germ line (Fig. 8C, D). Weak TIR1-1::mRuby expression was observed in the sperm and oocytes of the germline strains (Fig. 8C, D, Fig.8-figure supplement 1A-C").

To assess the efficacy of PEZO-1 degradation in these different tissues, we generated a strain with the *pezo-1* gene tagged at its N-terminus with GFP and at its C-terminus with the degron (GFP::PEZO-1::Degron). This strain was crossed with the strains expressing tir-1::mRuby driven by the three different promoters described above (Fig.8-figure supplement 2B-B''; D-D'', F-F''). GFP::PEZO-1::Degron strongly expresses at the plasma membrane of germline cells, oocytes, sperm, somatic sheath cells, and spermathecal cells (Fig.8-figure supplement 2A-A'', B-B'', D-D'', F-F''). The animals were exposed to either 0.25% ethanol as control or 2 mM auxin (indole-3-acetic acid, or IAA) for one generation and the GFP fluorescent intensity in their F1 progeny was analyzed. The strain expressing the degron interactor transgene $P_{eft\text{-}3}$*::tir-1::mRuby* led to a significant reduction of fluorescent intensity of GFP::PEZO-1::Degron at the sheath and spermathecal cells (Fig.8-figure supplement 2C-C''). While GFP fluorescence intensities in the germline and on oocyte in the germline-specific GFP::PEZO-1::Degron animals were 2-3 fold lower when the animals were exposed to auxin, however, the intensities was not affected in the somatic tissues (Fig.8-figure supplement 2E-E'', G-G'', H, I). Therefore, auxin-inducible degradation of GFP::PEZO-1::Degron in the different tissues is consistent with the TIR-1::mRuby expression pattern.

To further characterize the defects associated with the degradation of PEZO-1 in these different tissues, L4 animals were exposed to either 0.25% ethanol as control or 2 mM auxin and brood sizes were determined 0-60 hours post L4 (Day 1-3). Interestingly, the brood sizes were significantly reduced in each of the PEZO-1::Degron strains compared with control, regardless of the promoter used. However, the reduction in brood size was less severe than observed in the *pezo-1*^{ko} mutants (Fig. 8E, F, 2A). To ensure efficient degradation, we exposed animals to auxin for one generation and analyzed the brood size in their F1 progeny. This longer auxin exposure did not significantly enhance the reduction in brood size (data not shown).

Depletion of PEZO-1 in the somatic tissues, including spermathecal and sheath cells, led to a variety of ovulation defects (Fig.8-figure supplement 3A-I). Pinched oocytes were frequently observed during ovulation (N= 9/27, Fig.8-figure supplement 3I). A fraction of the pinched oocytes entered the spermatheca, while the rest were left in the oviduct (Fig.8-figure supplement 3C, D, I). Surprisingly, most of the pinched oocytes were successfully expelled into the uterus and underwent embryogenesis as smaller embryos (data not shown). Additionally, the process of oocyte entry into the spermatheca was frequently delayed or blocked (Fig.8-figure supplement 3E-I), suggesting the distal spermathecal valve remained closed. In experiments in which wildtype sperm were *in vivo* labeled as described earlier, and mated into control and somatic-specific PEZO-1::Degron hermaphrodites, nearly 90% of the labeled sperm reached the spermatheca (zone 3) and only a few labeled sperm were observed in the uterus (Fig. 8G, H, K). Notably, the ooplasmic uterine masses that we observed in our *pezo-1*^{ko} mutants were rarely observed in the somatic-specific degron strain.

Consistent with our male mating experiments, only 69% of the MitoTracker-labelled wildtype sperm accumulated at the spermatheca (zone 3) in the germline-specific PEZO-1::Degron animals exposed to the auxin (Fig. 8I-K). The remaining sperm were observed throughout the whole uterus (zone 1 and zone 2) after one hour of mating (Fig. 8I, J). Crushed oocytes were rarely observed in the uterus of the germline-specific PEZO-1::Degron animals, in which the sperm distribution assay was performed. Therefore, degradation of PEZO-1 in the germ line did not cause the severe uterine ooplasmic masses as we have observed for our *pezo-1*^{ko} mutants but did interfere with sperm navigation to the spermatheca, suggesting impaired attractant signaling. This is a more likely explanation since uterine ooplasmic masses are not a physical impediment to account for the defects in sperm migration.

Modeling human PIEZO genetic diseases in *C. elegans*

PIEZO patient-specific alleles, which are known to disrupt the normal physiological functioning of the cardiovascular, musculoskeletal, and blood systems in humans, were the motivation for examining the role of *pezo-1* in the tubular structures of *C. elegans.* Our studies with null alleles of *pezo-1* provide strong evidence that *pezo-1* is essential for normal *C. elegans* reproduction. It is therefore reasonable to model human monogenic diseases associated with *PIEZO1 and PIEZO2* mutations using the *C. elegans* reproductive system as a read-out of function. Individuals diagnosed with Dehydrated Hereditary Stomatocytosis (DHSt) were found to have a missense mutation in a conserved arginine residue (R2488Q) of PIEZO1. The orthologous residue

(R2718L/P) was also mutated in PIEZO2 in individuals with Distal Arthrogryposis type 5 (DA5) (Andolfo et al., 2013; Coste et al., 2013; Li et al., 2018; McMillin et al., 2014). Previous studies have shown that these arginine changes are functioning as gain-of-function mutations in their respective PIEZO protein (Albuisson et al., 2013; Coste et al., 2013; Li et al., 2018; McMillin et al., 2014). Sequence alignment indicated that R2405 in *C. elegans* PEZO-1 is the homologous arginine residue to both R2488 in human PEIZO1 and R2718 in human PIEZO2 (Fig. 9A). Using CRISPR/Cas9, we generated the patient-specific *PIEZO2* allele (p.R2718P) in *C. elegans,* named *pezo-1(R2405P)*. To compare this patient-specific allele with that of our null alleles, and to determine the phenotypic consequences of a patient-specific allele, homozygous animals carrying the *pezo-1(R2405P)* mutation were created. Such homozygotes displayed reproductive defects similar to the *pezo-1*^{ko} mutants, including reduced ovulation rates, ooplasmic uterine masses (Fig. 9B), and reduced brood sizes (Fig. 9C). Additionally, the phenotypes of *pezo-1(R2405P)* homozygotes were mildly enhanced in combination with *itr-1* RNAi and suppressed with *lfe-2* RNAi, consistent with our findings with *pezo-1*^{ko} mutants (Fig. 9D). Interestingly, similar to the rescue assay in *pezo-1 CΔ,* the reduced ovulation rate in *pezo-1(R2405P)* was also significantly rescued by *spe-9(hc52ts)* sperm, suggesting that this variant of *pezo-1* may similarly disrupt ovulation and sperm-to-sheath signaling, leading to self-sterility (Fig. 9E). Overall, these observations support the idea that *C. elegans* is an appropriate model system to study *PIEZO* diseases. Future suppressor screens with this and other *pezo-1* patient-specific alleles should help identify other genetic interactors.

Discussion

The PIEZO proteins are responsible for sensing mechanical stimuli during physiological processes. Most studies of PIEZOs have focused on electrophysiological assays in cultured cells. To take advantage of an *in vivo* system to investigate the developmental roles of the PIEZO channel in mechanotransduction, we have generated deletion alleles as well as a patient-specific allele in the sole *C. elegans pezo-1* gene. The *C. elegans* reproductive system is an attractive tubular system to study *PIEZO* function and mimic the *PIEZO* patient-specific alleles, which are known to disrupt the normal physiological functioning of the cardiovascular, musculoskeletal, and blood systems in humans (Albuisson et al., 2013; Alper, 2017; Andolfo et al., 2013; Bae et al., 2013). Though the PEZO-1 protein is broadly expressed throughout the animal, we focused on the reproductive system given its striking phenotypes. Utilizing different *pezo-1* mutants and the tissue-specific degradation of PEZO-1, our data indicate that dysfunction of *pezo-1* led to a significantly reduced brood size. This reduced brood size phenotype worsens with age. In *C. elegans*, the reproductive process incorporates a series of sequential events, including proper ovulation, fertilization, expulsion of the fertilized zygote into the uterus, and sperm navigation back to the spermatheca after each fertilization event, all of which are regulated by multiple inter-tissue signaling pathways.

PEZO-1 channel regulates ovulation and expulsion of the fertilized zygote possibly through maintaining cytosolic Ca^{2+} homeostasis

Ovulation is driven by the rhythmic and coordinated contraction of the gonadal sheath cells and opening of the spermathecal distal valve (McCarter et al., 1999). Similarly, expulsion of the fertilized zygote into the uterus is achieved by the contraction of the spermatheca and opening of the spermathecal-uterine valve. Mutations in the *pezo-1* gene cause quite dramatic effects on this entire process. We observed sheath cell defects such that the mature oocyte was not properly pushed into the spermatheca. In addition, spermathecal valve defects either inhibited proper entry of the oocyte into the spermatheca, or proper exit. In many cases, the oocyte was crushed as it progressed through the spermatheca, resulting in accumulation of ooplasm in the uterus. Genetic interactions between *pezo-1* mutants and *itr-1* or *lfe-2* RNAi support the idea that *pezo-1* may play a role in maintaining Ca^{2+} homeostasis during ovulation and zygote expulsion from the spermatheca. This is consistent with previous studies showing PIEZO1 responses to mechanical stimuli through Ca^{2+} signaling (He et al., 2018; Li et al., 2014). Based on present studies, we hypothesize a few possible pathways for a Ca^{2+}-mediated response to mechanical stimuli to which PEZO-1 may contribute. One possibility is that PEZO-1 may detect when cytosolic Ca^{2+} levels are extremely low and replenish the cell with extracellular Ca^{2+}, in a similar manner as the CRAC channel ORAI-1 (Lorin-Nebel et al., 2007). Consistent with this idea, our genetic data revealed an enhancement of the *pezo-1* phenotype upon CRAC channel *orai-1* RNAi, which is responsible for replenishing cytosolic Ca^{2+} (Fig. 4C). This suggests that PEZO-1 and ORAI-1 act in parallel pathways to replenish cytosolic Ca^{2+}. Previous studies identified the ER Ca^{2+} pump sarco/endoplasmic reticulum Ca^{2+} ATPase (SERCA) as an interacting partner of PIEZO1, which suppresses PIEZO1 activation

555 (Zhang et al., 2017). SERCA is essential for recycling Ca^{2+} into SR/ER Ca^{2+} stores,
556 which is an important process for maintaining Ca^{2+} homeostasis during tissue
557 contractility (Periasamy and Huke, 2001; Zwaal et al., 2001). PIEZO1 has been reported
558 to be involved in integrin activation to recruit the small GTPase R-Ras to the ER, which
559 promotes Ca^{2+} release from an intracellular store to the cytosol (McHugh et al., 2010).
560 These observations suggest that PEZO-1 may act as an ER Ca^{2+} channel to regulate
561 ER Ca^{2+} homeostasis. Lastly, normal spermathecal GCaMP fluorescence was observed
562 during the first three ovulations in *pezo-1* mutants, suggesting that other Ca^{2+} or
563 mechanosensitive channels may perform redundant functions during Ca^{2+} influx. One
564 alternative model could be that PEZO-1 acts in parallel to these Ca^{2+} regulators and yet
565 does not have a direct role in calcium homeostasis itself. Future studies will be required
566 to resolve the precise molecular effect of PEZO-1 on Ca^{2+} and understand how PEZO-1
567 regulates inter/intra cellular communication with/without Ca^{2+} and potentially how other
568 interacting partners coordinate during these processes.
569
570 **PEZO-1 channel is required for sperm navigation**
571 *C. elegans* employs multiple peptide and lipophilic hormones to coordinate
572 different tissues during reproduction. Ovulation is initiated by MSP (major sperm
573 proteins) signaling derived from sperm to trigger oocyte maturation and sheath cell
574 contraction (Kuwabara, 2003; McCarter et al., 1999; Miller, 2001). After each fertilization
575 event, oocytes secrete F-series prostaglandins (F-PGs) into the extracellular
576 environment of the reproductive tract and stimulate sperm attraction back to the
577 spermatheca (Hoang et al., 2013). Our observations revealed a strong expression of

PEZO-1 on the plasma membranes of both oocytes and sperm. Dysfunction of *pezo-1* causes a severe reduction of the ovulation rate and defective sperm navigation back to the spermatheca in aged animals. Male mating significantly rescued the very low ovulation rate in *pezo-1* mutants, as did the injection of purified fluorescently-tagged MSP. Furthermore, the sperm navigation defects were observed in the germline specific degradation of PEZO-1 animals, which showed less sperm successfully navigating back to the spermatheca. Collectively, depletion of PEZO-1 disrupted the ability of sperm to navigate back to the spermatheca, which may contribute to the reduced ovulation rate and defective sheath cell contraction.

Working Model

Our study supports the working model that PEZO-1 functions to promote the sheath cell contractions that push the oocyte into the spermatheca as the first step in ovulation (Fig. 10, step one). Simultaneously, PEZO-1 may play a role in sensing the sheath cell contractions and triggering the spermathecal distal valve to open to allow oocyte entry into the spermatheca. During fertilization, the distal and spermathecal-uterine valves have to remain closed, which likely is influenced by PEZO-1 (Fig. 10, step two). After fertilization, PEZO-1 regulates the spermathecal tissues and controls the sp-ut valve to trigger a series of events to expel the fertilized oocyte into the uterus. Lastly, PEZO-1 appears to function in the attraction of the sperm back into the spermatheca after being pushed out by the exiting of the newly fertilized oocyte (Fig. 10, step three). Thus, dysfunction of PEZO-1 may contribute to multiple defects in all these steps, including failure of oocyte entry into the spermatheca, the crushing of oocytes as

601 they transit through the ovary and spermatheca, and defective sheath-to-sperm
602 signaling perturbing the sperm from crawling back into the spermatheca after each
603 ovulation (Fig. 10). Future studies are underway to more precisely determine the PEZO-
604 1 function in each tissue (sheath, spermatheca, oocyte, and sperm) using even more
605 cell-specific promoters in the AID degradation system.
606
607 **Modeling PIEZO diseases in the *C. elegans* reproductive system**
608 Clinical reports indicate that either gain-of-function or loss-of-function mutations
609 in the human *PIEZO1* and *PIEZO2* cause a variety of physiological disorders (Alper,
610 2017). Interestingly, both gain-of-function and loss-of-function missense mutations were
611 identified in the same PIEZO disease, such as hydrops fetalis and lymphatic dysplasia.
612 However, the molecular mechanism underlying both extremes of PIEZO channel
613 dysfunction remains unclear (Alper, 2017). Complete knockout of *PIEZO1 and PIEZO2*
614 in mammalian models results in embryonic lethality and fetal cardiac defects,
615 suggesting an important role of PIEZO1/2 in embryonic and cardiac development
616 (Ranade et al., 2014; Zhang et al., 2019). However, lack of surviving homozygous
617 *PIEZO1/2* mutants in mammalian models make it challenging to investigate the PIEZO
618 function during embryogenesis and development.
619 A DA5 patient-specific allele in the *C. elegans pezo-1* gene displayed identical
620 reproductive phenotypes as our *pezo-1* deletion mutants, suggesting that this allele
621 must be loss-of-function. The observation that our *pezo-1* deletion strains and a putative
622 patient-specific gain-of-function mutation both lead to reproductive defects suggests that
623 either hypomorphic or hypermorphic PEZO-1 channel activity is harmful. Therefore, our

study demonstrates the usefulness of *C. elegans* as a model system to investigate PIEZO-derived human diseases.

Though the phenotypes described here in *C. elegans* do not exactly resemble those of the PIEZO-derived human diseases, there are similarities at the cellular level that may be relevant to the human diseases. Stretch-sensitive channels from the Piezo family are important for vascular development and lymphatic valve formation. In zebrafish, Piezo sense fluid flow to regulate both endothelial and smooth muscle cell maturation and forming heart valve development (Duchemin et al., 2019). In mice, PIEZO1 is required for the formation of lymphatic valves, a key structure for proper lymphatic circulation in the body (Nonomura et al., 2018). However, the mechanisms by which Piezo proteins operate and the proteins with which they interact remain unclear. In our study, we introduce a facile *in vivo* system for the study of PEZO-1 in the reproductive tract of *C. elegans*, a tubular tissue (spermatheca) with valves (spermatheca-uterine valve and distal valve) that must sense the incoming and exiting oocyte during ovulation and fertilization. How these structures form and function are likely conserved between humans and *C. elegans.*

The dramatic reduction in brood size that we observed in all our *pezo*-1 mutants will allow us to screen plausible chemical antagonists and agonists for PIEZO1 and PIEZO2 patient-specific alleles *in vivo*. In summary, we have demonstrated that the *C. elegans PIEZO1/2* ortholog, *pezo-1*, is required for efficient reproduction, and demonstrate the utility of *C. elegans* for the study of PIEZO functions. Future studies will determine if other patient-specific alleles disrupt ovulation and sperm navigational signaling. Using promoters with more restricted expression patterns, the tissue-specific

647 degradation system used in this report will also allow us to further dissect the
648 responsible cells or tissues that influence each of the phenotypes we observed in this
649 study. Future genetic and FDA-approved drugs screens will be used to identify putative
650 suppressors in *pezo-1* mutants. These screens may provide insightful approaches for
651 future clinical therapy.
652

Materials and Methods

C. elegans strains used in this study

C. elegans strains were maintained with standard protocols. Strain information is listed in Table 1. AG493, AG494 and AG495 were created by crossing AG487 (*pezo-1::Degron*) males with hermaphrodites containing *ieSi65 [Psun-1::tir1::sun-1 3'UTR + Cbr-unc-119(+)] II*, *ieSi57 [Peft-3::tir1::mRuby::unc-54 3'UTR + Cbr-unc-119(+)] II, and fxIs1[Ppie-1::tir1::mRuby] I*, respectively. We screened the F3 adults for the presence of the *tir-1::mRuby* transgene by microscopy and genotyped for the *pezo-1::Degron* by PCR. AG532 was created by crossing *pezo-1(av146 [gfp::pezo-1]) IV* males with the *unc-119(ed3); pwIs98 [YP170::tdimer2 + unc-119(+)] III* hermaphrodites containing YP170::tdimer2. F3 adults with YP170::tdimer2 were genotyped by PCR screening for the *pezo-1*^{KO} allele.

RNAi treatment

The RNAi feeding constructs were obtained from the Ahringer and Vidal libraries (Fraser et al., 2000; Rual et al., 2004). RNAi bacteria were grown until log phase was reached and spread on MYOB plates containing 1mM IPTG and 25 µg/ml carbenicillin and incubated overnight. To silence the target genes *itr-1* and *lfe-2*, mid-L4 hermaphrodites were picked onto plates with the IPTG-induced bacteria. Animals were grown on RNAi plates at 20°C for 36-60 hours. In order to improve the RNAi penetrance of *orai-1* and *sca-1*, L1 hermaphrodites were picked for RNAi feeding assays. Alternatively, mid-L4 hermaphrodites were incubated on the *orai-1* or *sca-1* RNAi plates for one generation, and F1 mid-L4 hermaphrodites were moved to fresh RNAi plates for brood size assays.

Brood size determinations and embryonic viability assays

Single mid-L4 hermaphrodites were picked onto 35 mm MYOB plates seeded with 10 µl of OP50 bacteria and allowed to lay eggs for 36 hours (plate one contains the brood size from 0-36 hours post mid-L4). The same hermaphrodite was moved to a new 35 mm MYOB plate to lay eggs for another 24 hours and were removed from the plate (this plate contains the brood size from 36-60 hours post mid-L4). Twenty-four hours after removing the moms, only fertilized embryos and larvae were counted for the brood size. Brood sizes were determined at 36 hours and 60 hours. Percentage of embryonic viability= (the number of hatched larva / the total brood size) *100%.

BODIPY 493/503 staining

BODIPY 493/503 (Invitrogen # D3922) was dissolved in 100% DMSO to 1 mg/ml. BODIPY stock was diluted by M9 to 6.7 µg/ml BODIPY (final concentration of DMSO was 0.8%) as the working stock. Hermaphrodites were washed in M9 three times and incubated in 6.7 µg/ml BODIPY for 20 minutes and washed again in M9 at least three times. All washes and incubations were performed in a concavity slide (ThermoFisher, # S99369). The stained hermaphrodites were anesthetized with 0.1% tricaine and 0.01% tetramisole in M9 buffer for 15-30 minutes. The anesthetized animals were then transferred to a 5% agarose pads for imaging. Image acquisition was captured by a Nikon 60 X 1.2 NA water objective with 1 µm z-step size.

Whole animal DAPI staining

Animals were washed in M9 in a concavity slide, and then transferred to 1µl of egg white/M9/azide on SuperFrost slides (Daigger # EF15978Z). Alternatively, animals were directly picked from plates into egg white/M9/azide, trying not to carry over too much

bacteria. With an eyelash, buffer around animals was spread out to a very thin layer, until animals are almost desiccated onto slide. Slides were immersed in a Coplin jar containing Carnoy's fixative and fixed for a minimum of 1.5 hours and as long as one week at room temperature or 4°C. Sequential ethanol (EtOH) rehydration was carried out in coplin jars containing about 50 ml of the following solutions for 2 minutes each: 90% EtOH in water, 70% EtOH in water, 50% EtOH in PBS, 25% EtOH in PBS, and PBS alone. Slides were then immersed in coplin jars containing DAPI stain (1 µg/ml) in PBS for 10 minutes. Slides were rinsed three times, 5 minutes each, in PBS. A drop of Vectashield mounting medium (#H-1500-10) was added as was a coverslip, followed by nail polish to seal the coverslip. Image acquisition was captured by a Nikon 60 X 1.2 NA water objective with 1 µm z-step size.

Yoda-1 dietary supplementation

Yoda1 (Tocris # 5586) was dissolved in DMSO to a stock concentration of 2.5 mM. This stock was added to 100 ml MYOB medium to a final concentration of 20 µM. Single mid-L4 hermaphrodites were picked onto 35 mm Yoda1 supplemented MYOB plates and control DMSO-only MYOB plates, each seeded with 10 µl of OP50 bacteria and allowed to lay eggs for 36 hours (plate one contains the brood from 0-36 hours post mid-L4). Each hermaphrodite was moved to a new 35 mm MYOB plate (with or without Yoda1) to lay eggs for another 24 hours and were removed from the plate (this plate contains the brood from 36-60 hours post mid-L4). Twenty-four hours after removing the moms, only fertilized embryos and larvae were counted to determine the brood size. Brood sizes were determined at 60 hours. Percentage of embryonic viability= (the number of hatched larva / the total number of hatched and unhatched animals) *100%.

Live imaging to determine ovulation rates

For imaging ovulation, animals were immobilized on 4% agar pads with anesthetic (0.1% tricaine and 0.01% tetramisole in M9 buffer). DIC image acquisition was captured by a Nikon 60 X 1.2 NA water objective with 1-2 μm z-step size; 10-15 z planes were captured. Time interval for ovulation imaging is every 45-60 seconds, and duration of imaging is 60-90 minutes. Ovulation rate= (number of successfully ovulated oocytes) / total image duration.

CRISPR design

We used the Bristol N2 strain as the wild type for CRISPR/Cas9 editing. The gene-specific 20-nucleotide sequences for crRNA synthesis were selected with help of a guide RNA design checker from Integrated DNA Technologies (IDT) (https://www.idtdna.com) and were ordered as 20 nmol or 4 nmol products from Dharmacon (https://dharmacon.horizondiscovery.com), along with tracrRNA. Repair template design followed the standard protocols (Paix et al., 2015; Vicencio et al., 2019). Approximately 30 young gravid animals were injected with the prepared CRISPR/Cas9 injection mix as described in the literature (Paix et al., 2015). *pezo-1 NΔ* and *pezo-1 CΔ* mutants were generated by CRISPR/Cas9 mixes that contained two guide RNAs at flanking regions of *pezo-1* coding regions. Heterozygous *pezo-1* deletion animals were first screened by PCR and then homozygosed in subsequent generations. mScarlet insertions at the *pezo-1* C-terminus were performed by Nested CRISPR (Vicencio et al., 2019). Homozygous *nest-1* edited animals were confirmed by PCR and restriction enzyme digestion and selected for the secondary CRISPR/Cas9 editing. Full-length mScarlet insertion animals were screened by PCR and visualized by

fluorescence microscopy. All homozygous animals edited by CRISPR/Cas9 were confirmed by Sanger sequencing (Eurofins). The detailed sequence information of the repair template and guide RNAs are listed in Table 2.

The short isoform deletion, *pezo-1(sy1398)*, was generated using Cas9 expressed from a plasmid (Friedland et al., 2013) and four guides (GAGAACTTGAATTCAATGG, AAGCTTCTTCCGTCTCCGG, GCAGTATTTGACCAACTGG, ATAAAACAAGGCAACCAGG) along with a *dpy-10* guide and repair oligo. These reagents were injected into young adult N2 animals and successful injections were identified by the presence of roller or dumpy progeny on the plate. Roller progeny were singled out and screened via PCR for the deletion mutation. The deletion was verified by Sanger sequencing using two external primers (CTCTCGCCTATCCACTTGAGCTTA, GGAAACAATTGAGCCGAGAATGGA) to amplify the region. This deletion should only disrupt expression of isoforms i and j (Fig.2-figure supplement 1B). The CRISPR-Cas9 STOP-IN mutant, *pezo-1(sy1199)*, was generated using purified Cas9 protein at 10 µg/µl concentration, a purified guide RNA near the mutation location (CCAGAAGCTCGTAAGCCAGG), and a single stranded DNA repair oligo containing three stop codons, one in every reading frame (underlined, cttatcgctgtttctgaaccagaagctcgtaagccGGGAAGTTTGTCCAGAGCAGAGGTGACTAAGTGATAAgctagcaggaggcactgaagaaacggatggtgatgaag). These reagents were injected into N2 young adults along with a *dpy-10* guide and repair oligo. Successful injections were identified by the presence of dumpy and roller progeny. 30 roller progeny were singled out from ‘jackpot’ plates (plates with a high incidence of dumpy and roller progeny) and

screened via PCR (GACAGGACTTTCCCGCCAACTTAA, ATCATTCGCCGATTGCACAAGTTG) and the presence of a NheI restriction site that was included in the repair oligo.

Male mating assay with Day 3 hermaphrodites

25-30 mid-L4 wildtype or *pezo-1* mutant hermaphrodites were isolated to a fresh growth plate for 60 hours (such animals should be Day 3 adults at this time). To ensure mating success, ~30 adult males and 10-15 Day 3 hermaphrodites were transferred onto a 35 mm MYOB plate seeded with 10-20 µl of OP50 bacteria and allowed to mate for 12 hours. The other 10-15 Day 3 hermaphrodites were singled and transferred to 35 mm MYOB plates seeded with 10 µl of OP50 bacteria as the controls. After the group mating, single mated hermaphrodites (72 hours post mid-L4) and 3-5 adult males were then transferred to a fresh 35 mm growth plate where mating could continue for another 24 hours. After 24 hours, the hermaphrodites (96 hours post mid-L4) and males were removed. The brood size (those embryos laid between 72-96 hours post mid-L4) and embryonic viability were determined 24 hours later after removal of all adults. Meanwhile, the broods from 60-96 hours post-mid L4 were also determined for the other 10-15 unmated Day 3 hermaphrodites that were kept on single plates as controls.

Mating assay with *fem-1* mutant

10-15 mid-L4 BA17 *fem-1(hc17ts)* hermaphrodites raised from embryos at the non-permissive temperature of 25°C were picked to mate with ~30 adult males for 12 hours at 25°C. Single mated hermaphrodites and 3-5 males were then transferred to a fresh 35 mm growth plate and allowed to mate for another 24 hours at 25°C before all adults

were removed from the plates. As control, 10-15 unmated BA17 hermaphrodites grown at 25°C were kept on single plates. The brood sizes and embryonic viability were determined 24 hours later. Alternatively, 10-15 L1 BA17 *fem-1(hc17ts)* hermaphrodites were isolated on a fresh growth plate and incubated at 25°C for 48 hours (young adult hermaphrodites). ~30 adult males and 10-15 BA17 young hermaphrodites were then transferred onto a 35 mm MYOB plate seeded with 10-20 ul of OP50 bacteria and allowed to mate for 12 hours at 25°C. Single mated hermaphrodites and 3-5 males were then transferred to a fresh 35 mm growth plate. After laying embryos for 24 hours, the hermaphrodites and males were removed. Meanwhile, the other same age 10-15 unmated Day 3 hermaphrodites were kept on single plates as the control. The brood size and embryonic viability were counted 24 hours later after removal of all adults. All the animals were incubated at 25°C during mating and propagation to ensure the penetration of the *fem-1(hc17ts)* phenotype.

Mating assay with *spe-9* mutant

10-15 hermaphrodites were picked to mate with ~30 AG521 [*spe-9(hc52ts)*] adult males for 12 hours at 25°C. Mated hermaphrodites were immobilized on 4% agar pads with anesthetic (0.1% tricaine and 0.01% tetramisole in M9 buffer) for ovulation rate assays. The acquisition of DIC images was performed by confocal imaging system (see below) with a Nikon 60 X 1.2 N with 1-2 μm z-step size and 10-15 z planes. Time interval for ovulation imaging is every 45-60 seconds, and duration of imaging is 60-90 minutes. Ovulation rate= (number of successfully ovulated oocytes) / total image duration.

Sperm distribution assay and mating assay

MitoTracker Red CMXRos (MT) (Invitrogen # M7512) was used to label male sperm following the protocol adapted from previous studies (Hoang et al., 2013; Kubagawa et al., 2006). MT was dissolved in 100% DMSO to 1 mM. About 100 males were transferred to a concavity slide (ThermoFisher, # S99369) with 150 µl 10 µM MT solution (diluted in M9 buffer). Males were incubated in the MT buffer for 2 hours and then transferred to fresh growth plates to recover overnight. The plates were covered by foil to prevent light exposure. About 30 males were placed with 10 anesthetized hermaphrodites (0.1% tricaine and 0.01% tetramisole in M9 buffer) on MYOB plates seeded with a 50-100 µl OP50 bacteria. After 30 minutes of mating, hermaphrodites were then isolated and allowed to rest on food for one hour. The mated hermaphrodites were then mounted for microscopy on 5% agarose pads with the anesthetic. Image acquisition was captured by a Nikon 60 X 1.2 NA water objective with 1 um z-step size. Quantification of sperm distribution in the uterus starts at the vulva and extends up to and includes the spermatheca. The sperm counted were throughout the gonad at a focal depth of about 30 µm. The whole uterus was divided into three zones. Zone 1 contains the vulva region, and Zone 3 contains the spermatheca. The number of sperm was manually counted within each zone. The distribution percentage= (the number in each zone) / (the total labeled sperm observed) * 100%. The quantified data contains at least 30 total stained sperm in the entire uterus. At least 3-7 mated hermaphrodites were counted in each mating assay, and experiments were repeated at least 3 times.

Auxin-inducible treatment in the degron strains

Animals were grown on bacteria-seeded MYOB plates containing auxin. The natural auxin indole-3-acetic acid (IAA) was purchased from Alfa Aesar (#A10556). IAA was

dissolved in ethanol as a 400 mM stock solution. Auxin was added to autoclaved MYOB agar when it cooled to about 50-60°C before pouring. MYOB plates containing the final concentration of auxin (1 or 2 mM) were used to test the degron-edited worms.

To efficiently degrade the target protein, L1 or L2 hermaphrodites were picked onto auxin plates. Animals were grown on the plates at 20°C for 36-60 hours for the brood size assay. Alternatively, mid-L4 hermaphrodites were incubated on the auxin plate for one generation, and F1 mid-L4 hermaphrodites were picked to a fresh auxin plate for the brood size assay or phenotypic imaging.

The microinjection of fluorescein-labeled MSP into aged *pezo-1 CΔ*

The microinjection of 101.6 μM NHS-Fluorescein-labeled MSP-142 into both aged (day 2, 48 hours post mid-L4) wildtype and *pezo-1 CΔ* hermaphrodites was performed as previously described (Miller, 2001). The injected worms recovered for 4 hours on MYOB plates with OP50 food before imaging. The acquisition of GFP and DIC images was performed by our confocal imaging system (see below) with 1-2 μm z-step size and 10-15 z planes. Time interval for ovulation imaging is every 45-60 seconds, and duration of imaging is 60-90 minutes. Ovulation rate= number of successfully ovulated oocytes/ total duration of imaging.

Microscopy

Live imaging was performed on a spinning disk confocal system that uses a Nikon 60 X 1.2 NA water objective, a Photometrics Prime 95B EMCCD camera, and a Yokogawa CSU-X1 confocal scanner unit. Images were acquired and analyzed by Nikon's NIS imaging software and ImageJ/FIJI Bio-formats plugin (National Institutes of Health) (Linkert et al., 2010; Schindelin et al., 2012). GCaMP3 images were also acquired by a

60×/1.40 NA oil-immersion objective on a Nikon Eclipse 80i microscope equipped with a SPOT RT39M5 sCMOS camera (Diagnostic Instruments, Sterling Heights, MI, USA) with a 0.63x wide field adapter, controlled by SPOT Advanced imaging software (v. 5.0) with Peripheral Devices and Quantitative Imaging modules. Images were acquired at 2448 × 2048 pixels, using the full camera chip, and saved as 8-bit TIFF files. Fluorescence excitation was provided by a Nikon Intensilight C-HGFI 130-W mercury lamp and shuttered with a Lambda 10-B SmartShutter (Sutter Instruments, Novato, CA), also controlled through the SPOT software. Single-channel GCaMP time-lapse movies were acquired using a GFP filter set (470/40× 495lpxr 525/50m) (Chroma Technologies, Bellows Falls, VT) at 1 frame per second, with an exposure time of 40-60 ms, gain of 8, and neutral density of 16.

GCaMP3 imaging acquisition and data processing

For all GCaMP3 imaging data, animals were immobilized on 7.5% agarose pads with 0.05 µm polystyrene beads and imaged using confocal microscopy as described above. Images were acquired every 1 second and saved as 16-bit TIFF files. DIC images were acquired every 3 seconds. Only successful embryo transits (embryos that were expelled through the sp-ut valve) were analyzed for this GCaMP3 study. The GCaMP3 metrics, including rising time and fraction over half max data, as well as the GCaMP3 intensity heat map were processed by the custom Fiji and Matlab coded platform (Bouffard et al., 2019). GCaMP3 kymograms were generated by custom Fiji code using the commands Image>Stacks>Reslice followed by Image>Stacks>Z Project (Average Intensity) (Bouffard et al., 2019). Only the very first three ovulations were imaged for each animal.

Detailed Processing and analysis of the GCaMP time series was performed exactly as described in (Bouffard et al., 2019).

Statistics

Statistical significance was determined by p value from an unpaired 2 tailed t-test. P-values: ns = not significant; * = <0.05; ** = <0.01, *** = <0.001; **** = <0.0001. Both the Shapiro-Wilk and Kolmogorov-Smirnov Normality test indicated that all data follow normal distributions.

Acknowledgments:

We thank the *Caenorhabditis* Genetics Center, which is funded by National Institutes of Health Office of Research Infrastructure Programs (P40OD010440), for providing strains for this study. We thank Dr. Orna Cohen-Fix for generously sharing the SP-12::GFP strain, and Dr. Harold Smith for sharing the BA17 *fem-1(hc17ts)* strain. We also thank Dr. David Greenstein for sharing fluorescein-tagged MSP and discussion about mating assays. We are grateful to the members of the Golden laboratory, Dr. Peter Kropp, Dr. Tao Cai, Rosie Bauer, Isabella Zafra, and Carina Graham for productive discussions and preparing reagents. We thank our summer intern Kyle Wilson for manuscript editing. We especially thank Dr. Harold Smith, Dr. Orna Cohen-Fix, Dr. Kevin O' Connell, Dr. Katherine McJunkin and Dan Konzman for critical inputs on the project and feedback on the manuscript. We thank all members of the Baltimore Worm Club for providing feedback and suggestions to our investigations.

Funding:

This work was supported, in part, by the Intramural Research Program of the National Institutes of Health, National Institute of Diabetes and Digestive and Kidney Diseases (X.B. and A.G.), National Institutes of Health, National Institute of General Medical Sciences (GM110268; J.B., A.L. and E.J.C.), and National Institutes of Health grants NIH R24 0D023041 and NIH R01 NS113119 (K.B. and P.W.S).

Figure Legends

Figure 1. *pezo*-1 is widely expressed in *C. elegans*

(A) Two fluorescent reporter genes were knocked-in to both the *pezo-1* N-terminus and C-terminus. (B) GFP::PEZO-1 is strongly expressed in multiple mechanosensitive tissues, such as the pharyngeal-intestinal valve, spermatheca, and vulva (red arrows). (C, E) GFP::PEZO-1 (green) is expressed in the plasma membrane of different staged embryos. (D) PEZO-1::mScarlet (magenta) localizes to the plasma membranes of embryos as well. (F) A schematic of the *C. elegans* gonad. (G-J) Both PEZO-1::mScarlet (magenta) and GFP::PEZO-1 (green) localize to reproductive tissues, such as the plasma membrane of the germline cells (G-I), somatic gonad (G-J), spermatheca (I; in white box), and sperm (J; red arrows). PEZO-1::mScarlet (magenta) also labels the spermatids that have not yet migrated into the spermatheca (small circles, white box in G) and the residual bodies not yet engulfed by the sheath cells (bigger circles, white box in G) (Huang et al., 2012). (K-O) Representative images of PEZO-1 localization during ovulation and fertilization. GFP::PEZO-1 (green) localizes to the sheath cell (white arrow) and the spermathecal distal valve (yellow arrow, K), which remains closed before ovulation. The oocyte ovulated and entered into the spermatheca (L) and stayed enclosed in the spermatheca until fertilization completed (M). During fertilization, GFP::PEZO-1 remained on the spermathecal-uterine (sp-ut) valve as indicated by a yellow arrow (M, N). The bag cells of the spermatheca also express GFP::PEZO-1 at this time (representative bag cells are marked by white arrows, L-N). After fertilization, the sp-ut valve opened (N, yellow arrow) and allowed the newly fertilized zygote to exit the constricting spermatheca (N, O). Constriction of the spermatheca pushes the

fertilized zygote into the uterus; sperm can be seen in the constricted spermatheca (O, yellow arrow). Black arrow above panel K shows the direction the embryo travels through the spermatheca from left to right. Timing of each step is labeled on the top right in minutes and seconds. Scale bars are indicated in each panel.

Figure 2. Deletions of the *pezo-1* gene cause a reduction in brood size

(A) Brood size was significantly reduced in both *pezo-1 NΔ* and *pezo-1 CΔ* animals when compared with wildtype and this reduction was most evident in older adult animals. (B) The percentage of viable embryos was reduced in the *pezo-1 CΔ* animals. (C) Dietary supplementation of a PIEZO1 channel specific activator Yoda1 in wildtype animals significantly reduced the brood size compared with control treatment, however brood size was not further reduced in *pezo-1 C*Δ when treated with Yoda1. (D, E) DIC images of the uteri of gravid adult animals. Wildtype animals had young embryos in their uteri (D), while only a large ooplasmic mass was observed in *pezo-1 CΔ* mutant uteri (E). (F) Quantification of the percentage of uteri with ooplasmic masses in wildtype and *pezo-1* deletion mutants. N2 is the wildtype strain. (G, H) DAPI staining demonstrated that multicellular embryos (white circles, G) were present in the uteri of wildtype animals, while only oocyte meiotic chromosomes (white circles and rectangle) were observed in the uteri of *pezo-1 CΔ* mutants (H; inset in top right white box shows an amplified image of the meiotic chromatin marked with a white rectangle). The yellow dotted lines indicate the boundaries of the uteri in panels G and H. (I, J) Only unfertilized oocytes and newly fertilized zygotes are permeable to BODIPY (green) in wildtype (WT) animals (I), while staining was observed throughout the entire uterine

mass (yellow circle, J) of *pezo-1 CΔ* animals. (K, L) An H2B::GFP transgene was crossed into our strains to visualize oocyte and sperm chromatin. (K) Sperm labeled by H2B::GFP (green cells in yellow circle) reside in the spermatheca (yellow circle) of Day 2 adults (48 hours post mid-L4). (L) Only oocyte debris (yellow circle) is left in the spermatheca of an age-matched *pezo-1 CΔ* mutant. (M) Quantification of sperm counts in both wildtype and *pezo-1 CΔ* hermaphrodites at different time windows. (N) Quantification of the oocyte ovulation rate of wildtype and *pezo-1 CΔ* adults at different ages. The oocyte ovulation rate was significantly reduced in the older *pezo-1 CΔ* mutant adults. P-values: * = 0.012 (M); ** = 0.0019 (B); ** = 0.0018 (C, blue); ** = 0.0054 (C, red); *** =0.0001 (C); **** <0.0001 (*t*-test).

Figure 3. PEZO-1 mutants exhibit severe ovulation defects

(A-E) Ovulation in wildtype animals. (A, B) Ovulation is initiated by oocyte (yellow dotted circle) entry into the spermatheca, which was labelled by the apical junctional marker DLG-1::GFP (green). (C) Fertilization occurs in the occupied spermatheca (yellow dotted circle). (D-E) After fertilization, the sp-ut valve (red arrows) opened immediately to allow the newly-fertilized zygote (yellow dotted circle) to exit the spermatheca and enter the uterus. (A'-E') Abnormal ovulation was observed in *pezo-1 CΔ* animals. Control of the spermathecal valves was aberrant (C'-E') during ovulation and the DLG-1::GFP labelled sp-ut valve (red arrow) never fully opened; the oocyte was crushed as it was expelled (E'). (F-M) Two examples of ovulation defects observed in the *pezo-1 C*Δ mutants. (F-I) The ovulating oocyte (white dotted circle) was pinched off by the spermathecal distal valve (red arrows, H). This oocyte never exited into the uterus. (J-

M) *pezo-1 CΔ* oocytes frequently failed to enter the spermatheca and were retained in the oviduct (M). Black arrow above panel A shows the direction the embryo travels through the spermatheca from left to right. All four image time series follow this same left to right orientation. Timing of each step is labeled on the bottom right in minutes and seconds. Scale bars are indicated in each panel.

Figure 4. *pezo-1* mutants show genetic interactions with cytosolic Ca^{2+} regulators

(A) *itr-1(RNAi)* reduced the brood size in *pezo-1 CΔ* animals. (B) In contrast, *lfe-2 (RNAi)* slightly rescued the smaller brood size in *pezo-1 CΔ* animals. (C) Depletion of both *orai-1* and *sca-1* by RNAi also enhanced the brood size reduction of *pezo-1 CΔ* mutants. P-values: * = 0.025 (C); ** = 0.0048 (A); *** = 0.0001 (B); **** <0.0001 (*t*-test).

Figure 5. PEZO-1 mutants show normal GCaMP3 fluorescence during ovulation

(A-E) mScarlet::PEZO-1 colocalizes with GCaMP3 that is driven by a spermatheca-specific promoter. These images represent the third ovulation for this spermatheca. (F-J') Time series frames from GCaMP3 recordings in the third ovulation of both wildtype animals (F-J) and *pezo-1 C*Δ animals (F'-J'). Ca^{2+} influx was quantified during ovulation and fertilization, as indicated by the intensity of GCaMP3 pixels (colored bar in F). (F, F') Oocyte entry into the spermatheca in wildtype and *pezo-1 CΔ.* (G, G') Oocytes in the spermatheca, (H, H') Ca^{2+} influx during fertilization, (I, I') intense Ca^{2+} influx as sp-ut valve closes to push newly-fertilized zygote into the uterus, and (J, J') the return to basal levels as the spermatheca prepares for the next ovulation. (K) Dwell time is a tissue function metric calculated as the time the oocyte resides in the spermatheca from

the closing of the distal valve to the opening of the sp-ut valve. (L, M) Calcium signaling metrics, fraction over half max (L), rising time (M) in *pezo-1* mutants showed normal calcium levels during ovulation compared with wild type (Bouffard et al., 2019). Black arrow above panel A shows the direction the embryo travels through the spermatheca from left to right. All three image time series follow this same left to right orientation. Timing of each step is labeled on the bottom right in minutes and seconds (A-E), or on the top left in seconds (F-J'). Scale bars are indicated in each panel.

Figure 6 Male sperm rescue the ovulation defects in *pezo-1* mutants

(A) Both *pezo-1 C*Δ and *N*Δ males are fertile and sire progeny when mated with *fem-1(hc17ts)* mutants (essentially female animals). (B) Mating with male sperm rescued fertility in Day 3 *pezo-1 CΔ* adults (72 hours post mid-L4). (C) The oocyte maturation and ovulation rate are very low in Day 3 *pezo-1 CΔ* mutant adults and oocytes accumulate in the proximal gonad arm (yellow dashed circle). (D) In contrast, the ovulation rates are recovered to high levels after mating with wildtype male sperm. Newly-fertilized embryos pushed the ooplasmic mass out of the uterus. Yellow asterisk indicates the spermatheca (C, D). **(**E) Quantification of the oocyte ovulation rate of wildtype and *pezo-1 CΔ* adults at different ages. *him-8(e1489)* and *spe-9 (hc52ts)* sperm significantly rescue ovulation rates in *pezo-1 CΔ* hermaphrodites even though they do not fertilize oocytes. (F, G) Injection of purified fluorescein-tagged MSP in the uteri of both wildtype and *pezo-1 C*Δ aged adults. Fluorescein-tagged MSP moved through the entire uterus to localize next to the spermatheca. The yellow dotted circle represents the spermatheca. The yellow arrows indicate the fluorescein-tagged MSP

(green) localized next to the spermatheca. (H) Quantification of the oocyte ovulation rate of wildtype and *pezo-1 C*Δ adults without or without injections of fluorescein-tagged MSP. P-values: **** <0.0001 (*t*-test). Scale bars are indicated in each panel.

Figure 7 Sperm guidance and navigation is disrupted in *pezo-1* mutants

(A) To quantify sperm migration, this illustration indicates the three zones that were scored for sperm distribution. Zone 3 is the spermatheca region and the space containing the +1 fertilized embryo (yellow dotted circles in panels B, D, F, H) while Zone 1 is the area closest to the vulva. Sperm distribution is measured 1 hour after males were removed from the mating plate. (B-I) The distribution of fluorescent male sperm labeled with MitoTracker in the three zones in both wildtype and *pezo-1* mutants 1 hour after the males were removed. Yellow asterisks indicate the vulva (C, E, G, I). Scale bars are indicated in each panel. (J) Quantification of sperm distribution values. Number of the scored uteri is shown above each of the bars. P-values: **** <0.0001 (*t*-test).

Figure 8 Tissue-specific degradation of PEZO-1 displays a reduced brood size and causes sperm navigational defects

(A) Schematic of the auxin-inducible degradation (AID) system. A degron tag was inserted at the 3' end of the *pezo-1* coding sequence using CRISPR/Cas9-mediated editing. (B) The *eft-3* promoter was used to drive TIR-1 expression in most or all somatic tissues, including the spermatheca and the sheath cells. TIR-1::mRuby driven by the germline specific promoters, *sun-1* and *pie-1,* is strongly expressed in the

germline and oocytes (C, D), and weakly expressed in the sperm (C, D, asterisk). (E, F) Brood size and embryonic viability were reduced in all degron strains when animals were treated with 2 mM auxin. Data are presented as the mean ± standard error from at least two independent experiments. (G-J) Sperm distribution 1 hour after male removal from mating plates. The germline specific PEZO-1::Degron hermaphrodites were mated with wildtype males for 30 minutes. The representative images show that *pezo-1* degradation in the germ line influences sperm distribution from the vulva (zone 1) to the spermatheca (zone 3). (K) Quantification of sperm distribution in the PEZO-1::Degron strains grown on plates with (+) or without (-) 2 mM auxin. P-values: * = 0.0146 (F); * = 0.016 (K); ** = 0.0030 (F); ** = 0.0053 (F); **** <0.0001 (E, K) (*t*-test). Scale bars are indicated in each panel.

Figure 9 A *PIEZO1* disease allele causes severe brood size reduction in *C. elegans*

(A) Sequence alignment showing arginine 2405 (R2405) in *C. elegans* PEZO-1 is highly conserved with human and mouse PIEZO1 and PIEZO2. (B) A conserved patient-specific allele, *pezo-1(R2405P),* was generated and causes uterine ooplasmic masses and (C) a severe reduction in brood size. (D) *itr-1(RNAi)* enhanced the brood size reduction of *pezo-1(R2405P)* mutants, while *lfe-2(RNAi)* slightly rescued the reduced brood size. (E) *spe-9(hc52ts)* sperm rescued the very low ovulation rate in *pezo-1(R2405P)* hermaphrodites. P-values: * = 0.0393 (D); ** = 0.0079 (D); **** <0.0001 (C) (*t*-test).

Figure 10 Working Model for PEZO-1 during ovulation

Step One: PEZO-1 regulates somatic sheath cells and the spermathecal distal valve to push the oocyte into the spermatheca. Once a matured oocyte is ready for ovulation, PEZO-1 (red trapezoids) on the somatic sheath cells (yellow) triggers the contraction of the sheath to push the oocyte into the dilating spermatheca, through the distal valve. Meanwhile, the activated PEZO-1 (red trapezoids) on the distal valve (yellow) keeps the valve open and allows oocyte entry the spermatheca (green). Step Two: during fertilization, the PEZO-1 (red trapezoids) coordinates both distal (yellow) and spermathecal-uterine valves (yellow) to remain closed for 3-5 minutes. Step Three: After fertilization, PEZO-1 (red trapezoids) is activated on the spermathecal bag cells (yellow) and the sp-ut valve (yellow) to trigger a series of mechanical events (including spermathecal contractions and sp-ut valve opening) to expel the fertilized oocyte into the uterus (green). After oocyte entry into the uterus, we speculate that the PEZO-1 (red trapezoids) on the oocyte (far left) also functions to attract the sperm (green cells) back to the spermatheca. The precise mechanism of how PEZO-1 regulates sperm attraction remains unknown. Dysfunction of PEZO-1 causes the oocytes to be crushed as they are pushed into (Step One) and expelled from the spermatheca (Step Three). The yellow represents the tissues under mechanical tension at each step during ovulation. PEZO-1 likely functions at the plasma membrane to sense the mechanical stimuli and trigger intracellular signaling. The black arrows indicate the direction of extracellular cation influx when PEZO-1 channels are activated.

Figure 1- figure supplement 1. PEZO-1 is expressed in multiple tissues throughout development

(A) There are 14 mRNA isoforms encoded by *pezo-1*. Isoforms i-l encode the six short forms of *pezo-1* (red asterisks). The 5'-3' orientation is right to left. (B-G) Both PEZO-1::mScarlet (magenta) and GFP::PEZO-1 (green) express in a variety of cell types, including pharyngeal neurons (B, white arrows), pharyngeal-intestinal valve (C), male tail, including sensory rays (magenta), fan (green), cloaca/spicules (green) (D), vulva (E), intestinal cells (F) and seam cells (G). Scale bars are indicated in each panel. Illustration in panel A was taken from WormBase (https://wormbase.org).

Figure 2- figure supplement 1. Verification of CRISPR/Cas9 generated deletions in *pezo-1* knockout animals

(A) Representative PCR gel from genotyping single animals for *pezo-1 C*Δ *k*nockout candidates. A positive homozygous knockout line is labeled with a red asterisk. Three primers (two that flank the deletion and one internal) were used to test the homozygosity of candidate *pezo-1* deletion animals. Amplicon size of a homozygous deletion with both flanking primers is 450 bp (labeled -/-). In wild type, an 879bp PCR product was able to be amplified by one flanking primer and the internal primer (labelled +/+). Heterozygous animals contain both of the PCR products (labeled +/-). (B) Schematic of the 14 mRNA isoforms and the position of the three deletion alleles used in this study and which isoforms they should affect. The STOP-IN line is also shown as an insertion in the beginning of exon 27. The 5'-3' orientation is right to left. (C) Full deletion allele and four other alleles generated for this study also had reduced brood

sizes; full deletion mutant *pezo-1(av240),* a N-terminal mutant *pezo-1(av144),* a C-terminal mutant *pezo-1(av149)* a stop-in mutant *pezo-1(sy1199)* and a small deletion allele *pezo-1(sy1398)* in isoforms I and J. (D) The reduction in brood size of *pezo-1* deletion animals was enhanced when the animals were grown at 25°C. (E) Quantification of the percentage of uteri with ooplasmic masses in *pezo-1(sy1199)* and *pezo-1(sy1398)* mutants. P-values: *** =0.0003 (C); ** = 0.0021 (D); *** =0.0002 (D); **** <0.0001 (*t*-test). Illustration in panel B was taken from WormBase (https://wormbase.org).

Figure 5- figure supplement 1. Normal calcium signaling was observed in the spermathecal cells in *pezo-1* mutants

(A, B) GCaMP3 time series of normalized average pixel intensity from a single oocyte transit recording over the same spatial frame and time. (C) Heat map of GCaMP3 normalized average pixel intensity (F/F_0) versus time series during ovulation from seven oocyte transit recordings in both wildtype and *pezo-1 CΔ* mutants. Color bars represents the gradient of the normalized average pixel intensity (F/F_0). (D, E) Representative kymograms of GCaMP3 in both wildtype and *pezo-1 CΔ* mutants. Color bars represents the gradient of the fluorescence intensity.

Figure 6- figure supplement 1. Male sperm rescue the fecundity in *pezo-1 CΔ* female

(A) Brood size was significantly reduced in *pezo-1 CΔ* females when compared with *fem-1(hc17)* females only at permissive temperature (15°C). (B) Quantification of

Mito tracker stained male sperm in the female uteri after mating for 30 minutes. (C) Both *pezo-1 C*Δ and wildtype males sire progeny when mated with *fem-1(hc17ts)* mutants (essentially female animals) and *pezo-1 CΔ* female at non-permissive temperature (25°C). However, the number of cross progeny was greatly reduced in the *pezo-1 C*Δ female. (D) Fertilization ratio [(laid embryos/stained sperm) *100%] in different females. (E) Quantification of sperm distribution in the *pezo-1 C*Δ female after mating 30 minutes. P-values: * = 0.031 (B); ** = 0.0014 (A); *** = 0.0001 (D); **** <0.0001 (A, D, E) (*t*-test).

Figure 8- figure supplement 1. Expression pattern of *tir-1::mRuby* in reproductive tissues

(A-A'') The *eft-3* promoter was used to drive TIR-1 expression in most or all somatic tissues, including the spermatheca but not in the sperm [bottom insert (A), dotted circle]. Strong GFP autofluorescence is observed in the sperm cytosol [bottom insert (A), A'']. (B-C'') TIR-1::mRuby driven by the germline specific promoters, *sun-1* and *pie-1,* is strongly expressed in the germline and oocytes (B-B', C-C') and weakly expressed in the sperm (dotted circles in the bottom panels under B and C).

Figure 8- figure supplement 2. Tissue-specific degradation of PEZO-1 displays a reduced GFP::PEZO-1 fluorescence in each tissue expressing *tir-1::mRuby.*

(A-A'') GFP::PEZO-1::Degron localized to reproductive tissues, such as the plasma membrane of the germline cells, oocyte, somatic sheath cells (yellow arrow, A, A''), spermatheca (yellow arrow, A, A'') and sperm. (B-B'') TIR-1::mRuby driven by the

somatic tissue specific promoter, *eft-3,* is strongly expressed in the somatic sheath cells and spermatheca. (C-C'', H-I) Fluorescent signals of GFP::PEZO-1::Degron at spermatheca and somatic sheath cells significantly reduced when animals were treated with 2 mM auxin. However, fluorescent signals of GFP::PEZO-1::Degron at germline cells, oocyte and sperm are not affected. (D-E'') TIR-1::mRuby driven by the germline specific promoters, *sun-1* and *pie-1,* is strongly expressed in the germline and oocytes (D', E', F, G'). Fluorescent signals of GFP::PEZO-1::Degron in germline cells and oocytes was significantly reduced (D-G, D''-G'', H-I), while the expression level of GFP::PEZO-1::Degron in somatic tissues is not affected (D-G, D''-G'', H-I). (H-I) Quantification of the fluorescent signals of GFP::PEZO-1::Degron at the different conditions. P-values: **** <0.0001 (*t*-test).

Figure 8- figure supplement 3. Somatic-tissue specific degradation of PEZO-1 causes severe ovulation defects

(A-H) Abnormal ovulations were observed in the somatic tissue specific PEZO-1::Degron animals. Shown are two different ovulation events. (A, E) Ovulation initiated by oocyte (yellow dotted circle) entry into the spermatheca. Spermathecal distal valve (red arrows) was defective (B, C, E-H) and either pinched off the oocyte when it attempted to enter the spermatheca (B-D) or failed to open and block/delayed the entry of the oocyte into the spermatheca (yellow asterisks) (E-H). Timing of each step is labeled in each panel in minutes and seconds. (I) Quantification of the oocyte ovulation rate and ovulation defects in the *Peft-3::tir-1; pezo-1::Degron* animals with or without 2 mM auxin. Scale bars are indicated in each panel.

Video 1. PEZO-1 expression pattern during ovulation

Ovulation imaged in the genome-edited animals expressing GFP::PEZO-1 (green). Yellow arrow in right panel indicates GFP::PEZO-1 expression on the spermathecal valves. White arrows in right panel indicate GFP::PEZO-1 expression on the bag cells. After fertilization, GFP::PEZO-1 labeled sperm crawled back to the spermatheca. Left panel shows the merged channel of DIC (grey) with GFP (green). Right panel indicates the GFP (green) channel only. Images are single z planes taken every 2 seconds. Timing is indicated in lower right. Playback rate is 15 frames/second. Scale bar is indicated in left panel.

Video 2. Crushed oocyte phenotype frequently occurs in the *pezo-1 CΔ* mutant

Time-lapse video recording showing a wildtype oocyte (top panel) entering into the spermatheca and completing fertilization in 5 minutes. The constricted spermatheca smoothly expels the oocyte into the uterus. White arrows in top panel indicate opening spermathecal valve. In the bottom panel, the *pezo-1 CΔ* oocyte successfully enters the spermatheca, but the oocyte is crushed by the sp-ut valve and the ooplasmic debris is observed in the uterus. Yellow arrows in bottom panel indicate the spermathecal valve. Images are single z planes taken every 2 seconds. Timing is indicated in lower right. Playback rate is 15 frames/second. Scale bars are indicated in each panel.

Video 3. The sp-ut valve fails to open during spermathecal contraction

Time-lapse recordings on left are of DIC and GFP. Recordings on right are only of GFP. Oocyte entry occurs from the left at the 15 second mark. The spermatheca was labelled by the apical junctional marker DLG-1::GFP. In the wild type (top panels), the sp-ut valve (white arrow) opened immediately to allow the oocyte to be expelled into the uterus (on right). However, in *pezo-1 CΔ* (bottom panels), the DLG-1::GFP labelled sp-ut valve (white arrow) never fully opened, the oocyte was crushed as it was expelled, and ooplasmic debris was pushed out into the uterus. Images are single z planes taken every 3 seconds. Timing is indicated in lower right. Playback rate is 15 frames/second. Scale bars are indicated in each DIC panel.

Video 4. Spermatheca dilation is defective in *pezo-1* mutants

Time-lapse video recording (DIC). Oocyte entry occurs from the left at the 35 second mark. The distal valve was not able to completely close and the oocyte was pinched. One portion of the broken oocyte was left in the spermatheca, the other portion remains in the oviduct (white arrows, left panel). Images are single z planes taken every 2 seconds. Timing is indicated in lower left. Playback rate is 15 frames/second. Scale bar is indicated in lower right.

Video 5. Sheath cell contraction is defective in *pezo-1* mutants

Time-lapse video recording (DIC). Oocyte that fails to enter the spermatheca after a few attempts. Sheath cells failed to contract and push the oocyte into the spermatheca (on the right) and oocyte moves left, back into the oviduct. Images are single z planes taken every 2 seconds. Timing is indicated in lower right. Playback rate is 15 frames/second. Scale bar is indicated in lower left.

Video 6. mScarlet::PEZO-1 colocalizes with spermathecal-specific GCaMP3

Example of the colocalization of mScarlet::PEZO-1 (magenta) with the Pfln-1::GCaMP3 transgene (green) in the spermathecal cells in a wildtype animal. Top left recording shows the merged channel of DIC (grey), mScarlet::PEZO-1 (magenta) and the *Pfln-1::GCaMP3* transgene (green). Top right panel lacks the DIC channel. Bottom left recording shows just the mScarlet::PEZO-1 expression pattern during ovulation. Bottom right indicates that Pfln-1::GCaMP3 only displays the changes of GCaMP3 intensity, which is indicative of calcium influx. Images were acquired in a single z plane every 2 seconds. Timing is indicated in lower right panel. Playback rate is 30 frames/second. Scale bars are indicated in each panel.

Video 7. Normal GCaMP3 influx was observed in *pezo-1* mutants

Examples of GCaMP3 recordings of embryo transits in wildtype (left panels) and *pezo-1 CΔ* (right panels) animals. Recordings were temporally aligned to the start of oocyte entry at 50 seconds. GCaMP3 normalized average pixel intensity (F/F_0, top, Y-axis) versus GCaMP3 time (top, X-axis) generated from GCaMP3 recordings with highlighted metrics on the top of the tracings. Dwell time is a tissue function metric that represents the duration from the closing of the distal valve to the opening of the sp-ut valve, rising time is a calcium signaling metric measuring the time from the opening of the distal valve to the first time point where the time series reaches half maximum of GCaMP3 intensity, and fraction over half max is a calcium signaling metric, which measures the duration of the dwell time over the GCaMP3 half-maximal value divided by the total

dwell time. Images were acquired in a single z plane every 1 second. Timing is indicated in top left of each bottom panel. Playback rate is 30 frames/second. Scale bars are indicated in each panel.

Figure1-source data1. Number of independent samples were collected for *pezo-1* expression pattern in *C. elegans*

Figure 2- source data 1. Quantificaiton data of brood size, the percentage of viable embryos and sperm counts of *pezo-1* mutants compared with wild-type.

Figure 2-figure supplement source data 1. Quantificaiton data of brood size and the percentage of viable embryos of *pezo-1* mutants compared with wild-type.

Figure 3- source data 1. Number of independent samples were collected for imaging ovualiton defects in *pezo-1* mutants.

Figure 4- source data1. Quantification of brood size for genetic interaction of *pezo-1* mutants with RNAi depletion of calcium regulators

Figure5-source data1. Quantification of calcium metrics in *pezo-1* mutants and wild-type.

Figure 6-source data1. Quantification of sire progeny in different mating assays.

Figure 6-figure supplement 1-source data1. Quantification of sire progeny and sperm count in different mating assays.

Figure 7-source data1. Quantification of sperm count in sperm distribution assays.

Figure 8-source data1. Quantification of brood size and sperm counts in each AID strains.

Figure 8-figure supplement 2-source data1. Quantification of the fluorescent intensity of GFP-PEZO-1::Degron at different conditions.

Figure 9-source data1. Quantification of brood size in patient-specific allele *pezo-1(R2405P)* and the genetic interaction of *pezo-1(R2405P)* with RNAi depletion of calcium regulators.

Bibliography

Albuisson, J., Murthy, S.E., Bandell, M., Coste, B., Louis-Dit-Picard, H., Mathur, J., Feneant-Thibault, M., Tertian, G., de Jaureguiberry, J.P., Syfuss, P.Y., Cahalan, S., Garcon, L., Toutain, F., Simon Rohrlich, P., Delaunay, J., Picard, V., Jeunemaitre, X., Patapoutian, A., 2013. Dehydrated hereditary stomatocytosis linked to gain-of-function mutations in mechanically activated PIEZO1 ion channels. Nat Commun 4, 1884.

Alper, S.L., 2017. Genetic Diseases of PIEZO1 and PIEZO2 Dysfunction. Curr Top Membr 79, 97-134.

Andolfo, I., Alper, S.L., De Franceschi, L., Auriemma, C., Russo, R., De Falco, L., Vallefuoco, F., Esposito, M.R., Vandorpe, D.H., Shmukler, B.E., Narayan, R., Montanaro, D., D'Armiento, M., Vetro, A., Limongelli, I., Zuffardi, O., Glader, B.E., Schrier, S.L., Brugnara, C., Stewart, G.W., Delaunay, J., Iolascon, A., 2013. Multiple clinical forms of dehydrated hereditary stomatocytosis arise from mutations in PIEZO1. Blood 121, 3925-3935, S3921-3912.

Bae, C., Gnanasambandam, R., Nicolai, C., Sachs, F., Gottlieb, P.A., 2013. Xerocytosis is caused by mutations that alter the kinetics of the mechanosensitive channel PIEZO1. P Natl Acad Sci USA 110, E1162-E1168.

Bouffard, J., Cecchetelli, A.D., Clifford, C., Sethi, K., Zaidel-Bar, R., Cram, E.J., 2019. The RhoGAP SPV-1 regulates calcium signaling to control the contractility of the Caenorhabditis elegans spermatheca during embryo transits. Mol Biol Cell 30, 907-922.

Bui, Y.K., Sternberg, P.W., 2002. Caenorhabditis elegans inositol 5-phosphatase homolog negatively regulates inositol 1,4,5-triphosphate signaling in ovulation. Mol Biol Cell 13, 1641-1651.

Clandinin, T.R., DeModena, J.A., Sternberg, P.W., 1998. Inositol trisphosphate mediates a RAS-independent response to LET-23 receptor tyrosine kinase activation in C. elegans. Cell 92, 523-533.

Coste, B., Houge, G., Murray, M.F., Stitziel, N., Bandell, M., Giovanni, M.A., Philippakis, A., Hoischen, A., Riemer, G., Steen, U., Steen, V.M., Mathur, J., Cox, J., Lebo, M., Rehm, H., Weiss, S.T., Wood, J.N., Maas, R.L., Sunyaev, S.R., Patapoutian, A., 2013. Gain-of-function mutations in the mechanically activated ion channel PIEZO2 cause a subtype of Distal Arthrogryposis. Proc Natl Acad Sci U S A 110, 4667-4672.

Coste, B., Mathur, J., Schmidt, M., Earley, T.J., Ranade, S., Petrus, M.J., Dubin, A.E., Patapoutian, A., 2010. Piezo1 and Piezo2 are essential components of distinct mechanically activated cation channels. Science 330, 55-60.

Coste, B., Xiao, B., Santos, J.S., Syeda, R., Grandl, J., Spencer, K.S., Kim, S.E., Schmidt, M., Mathur, J., Dubin, A.E., Montal, M., Patapoutian, A., 2012. Piezo proteins are pore-forming subunits of mechanically activated channels. Nature 483, 176-181.

Cram, E.J., 2014. Mechanotransduction in C. elegans morphogenesis and tissue function. Prog Mol Biol Transl Sci 126, 281-316.

Cram, E.J., 2015. Mechanotransduction: feeling the squeeze in the C. elegans reproductive system. Curr Biol 25, R74-R75.

Del Marmol, J.I., Touhara, K.K., Croft, G., MacKinnon, R., 2018. Piezo1 forms a slowly-inactivating mechanosensory channel in mouse embryonic stem cells. Elife 7.

Doniach, T., Hodgkin, J., 1984. A Sex-Determining Gene, Fem-1, Required for Both Male and Hermaphrodite Development in Caenorhabditis-Elegans. Developmental Biology 106, 223-235.
Duchemin, A.L., Vignes, H., Vermot, J., 2019. Mechanically activated piezo channels modulate outflow tract valve development through the Yap1 and Klf2-Notch signaling axis. Elife 8.
Fraser, A.G., Kamath, R.S., Zipperlen, P., Martinez-Campos, M., Sohrmann, M., Ahringer, J., 2000. Functional genomic analysis of C. elegans chromosome I by systematic RNA interference. Nature 408, 325-330.
Friedland, A.E., Tzur, Y.B., Esvelt, K.M., Colaiacovo, M.P., Church, G.M., Calarco, J.A., 2013. Heritable genome editing in C. elegans via a CRISPR-Cas9 system. Nat Methods 10, 741-743.
Gnanasambandam, R., Bae, C., Gottlieb, P.A., Sachs, F., 2015. Ionic Selectivity and Permeation Properties of Human PIEZO1 Channels. PLoS One 10, e0125503.
Greenstein, D., 2005. Control of oocyte meiotic maturation and fertilization. WormBook, 1-12.
Han, S.M., Cottee, P.A., Miller, M.A., 2010. Sperm and oocyte communication mechanisms controlling C. elegans fertility. Dev Dyn 239, 1265-1281.
Harris, T.W., Arnaboldi, V., Cain, S., Chan, J., Chen, W.J., Cho, J., Davis, P., Gao, S., Grove, C.A., Kishore, R., Lee, R.Y.N., Muller, H.M., Nakamura, C., Nuin, P., Paulini, M., Raciti, D., Rodgers, F.H., Russell, M., Schindelman, G., Auken, K.V., Wang, Q., Williams, G., Wright, A.J., Yook, K., Howe, K.L., Schedl, T., Stein, L., Sternberg, P.W., 2019. WormBase: a modern Model Organism Information Resource. Nucleic Acids Res.
He, L., Si, G., Huang, J., Samuel, A.D.T., Perrimon, N., 2018. Mechanical regulation of stem-cell differentiation by the stretch-activated Piezo channel. Nature 555, 103-106.
Hoang, H.D., Prasain, J.K., Dorand, D., Miller, M.A., 2013. A heterogeneous mixture of F-series prostaglandins promotes sperm guidance in the Caenorhabditis elegans reproductive tract. PLoS Genet 9, e1003271.
Huang, J., Wang, H.B., Chen, Y.Y., Wang, X.C., Zhang, H., 2012. Residual body removal during spermatogenesis in C. elegans requires genes that mediate cell corpse clearance. Development 139, 4613-4622.
Johnston, W.L., Krizus, A., Dennis, J.W., 2010. Eggshell chitin and chitin-interacting proteins prevent polyspermy in C. elegans. Curr Biol 20, 1932-1937.
Kelley, C.A., Cram, E.J., 2019. Regulation of Actin Dynamics in the C. elegans Somatic Gonad. J Dev Biol 7.
Kimble, J., Hirsh, D., 1979. The postembryonic cell lineages of the hermaphrodite and male gonads in Caenorhabditis elegans. Dev Biol 70, 396-417.
Kovacevic, I., Orozco, J.M., Cram, E.J., 2013. Filamin and phospholipase C-epsilon are required for calcium signaling in the Caenorhabditis elegans spermatheca. PLoS Genet 9, e1003510.
Kubagawa, H.M., Watts, J.L., Corrigan, C., Edmonds, J.W., Sztul, E., Browse, J., Miller, M.A., 2006. Oocyte signals derived from polyunsaturated fatty acids control sperm recruitment in vivo. Nat Cell Biol 8, 1143-1148.
Kuwabara, P.E., 2003. The multifaceted C-elegans major sperm protein: an ephrin signaling antagonist in oocyte maturation. Gene Dev 17, 155-161.
Li, J., Hou, B., Tumova, S., Muraki, K., Bruns, A., Ludlow, M.J., Sedo, A., Hyman, A.J., McKeown, L., Young, R.S., Yuldasheva, N.Y., Majeed, Y., Wilson, L.A., Rode, B., Bailey, M.A., Kim, H.R., Fu, Z., Carter, D.A., Bilton, J., Imrie, H., Ajuh, P., Dear, T.N., Cubbon, R.M., Kearney, M.T., Prasad,

R.K., Evans, P.C., Ainscough, J.F., Beech, D.J., 2014. Piezo1 integration of vascular architecture with physiological force. Nature 515, 279-282.
Li, J., Hou, B., Tumova, S., Muraki, K., Bruns, A., Ludlow, M.J., Sedo, A., Hyman, A.J., McKeown, L., Young, R.S., Yuldasheva, N.Y., Majeed, Y., Wilson, L.A., Rode, B., Bailey, M.A., Kim, H.R., Fu, Z.J., Carter, D.A.L., Bilton, J., Imrie, H., Ajuh, P., Dear, T.N., Cubbon, R.M., Kearney, M.T., Prasad, K.R., Evans, P.C., Ainscough, J.F.X., Beech, D.J., 2015. Piezo1 Integration of Vascular Architecture with Physiological Force. Faseb J 29.
Li, S., You, Y., Gao, J., Mao, B., Cao, Y., Zhao, X., Zhang, X., 2018. Novel mutations in TPM2 and PIEZO2 are responsible for distal arthrogryposis (DA) 2B and mild DA in two Chinese families. BMC Med Genet 19, 179.
Linkert, M., Rueden, C.T., Allan, C., Burel, J.M., Moore, W., Patterson, A., Loranger, B., Moore, J., Neves, C., Macdonald, D., Tarkowska, A., Sticco, C., Hill, E., Rossner, M., Eliceiri, K.W., Swedlow, J.R., 2010. Metadata matters: access to image data in the real world. J Cell Biol 189, 777-782.
Lorin-Nebel, C., Xing, J., Yan, X.H., Strange, K., 2007. CRAC channel activity in C-elegans is mediated by Orai1 and STIM1 homologues and is essential for ovulation and fertility. J Physiol-London 580, 67-85.
Lukacs, V., Mathur, J., Mao, R., Bayrak-Toydemir, P., Procter, M., Cahalan, S.M., Kim, H.J., Bandell, M., Longo, N., Day, R.W., Stevenson, D.A., Patapoutian, A., Krock, B.L., 2015. Impaired PIEZO1 function in patients with a novel autosomal recessive congenital lymphatic dysplasia. Nat Commun 6, 8329.
McCarter, J., Bartlett, B., Dang, T., Schedl, T., 1999. On the control of oocyte meiotic maturation and ovulation in Caenorhabditis elegans. Dev Biol 205, 111-128.
McHugh, B.J., Buttery, R., Lad, Y., Banks, S., Haslett, C., Sethi, T., 2010. Integrin activation by Fam38A uses a novel mechanism of R-Ras targeting to the endoplasmic reticulum. J Cell Sci 123, 51-61.
McKnight, K., Hoang, H.D., Prasain, J.K., Brown, N., Vibbert, J., Hollister, K.A., Moore, R., Ragains, J.R., Reese, J., Miller, M.A., 2014. Neurosensory perception of environmental cues modulates sperm motility critical for fertilization. Science 344, 754-757.
McMillin, M.J., Beck, A.E., Chong, J.X., Shively, K.M., Buckingham, K.J., Gildersleeve, H.I., Aracena, M.I., Aylsworth, A.S., Bitoun, P., Carey, J.C., Clericuzio, C.L., Crow, Y.J., Curry, C.J., Devriendt, K., Everman, D.B., Fryer, A., Gibson, K., Giovannucci Uzielli, M.L., Graham, J.M., Jr., Hall, J.G., Hecht, J.T., Heidenreich, R.A., Hurst, J.A., Irani, S., Krapels, I.P., Leroy, J.G., Mowat, D., Plant, G.T., Robertson, S.P., Schorry, E.K., Scott, R.H., Seaver, L.H., Sherr, E., Splitt, M., Stewart, H., Stumpel, C., Temel, S.G., Weaver, D.D., Whiteford, M., Williams, M.S., Tabor, H.K., Smith, J.D., Shendure, J., Nickerson, D.A., University of Washington Center for Mendelian, G., Bamshad, M.J., 2014. Mutations in PIEZO2 cause Gordon syndrome, Marden-Walker syndrome, and distal arthrogryposis type 5. Am J Hum Genet 94, 734-744.
Miller, M.A., 2001. A sperm cytoskeletal protein that signals oocyte meiotic maturation and ovulation (vol 292, pg 2144, 2001). Science 292, 639-639.
Miller, M.A., Ruest, P.J., Kosinski, M., Hanks, S.K., Greenstein, D., 2003. An Eph receptor sperm-sensing control mechanism for oocyte meiotic maturation in Caenorhabditis elegans. Genes Dev 17, 187-200.

Murthy, S.E., Dubin, A.E., Patapoutian, A., 2017. Piezos thrive under pressure: mechanically activated ion channels in health and disease. Nat Rev Mol Cell Biol 18, 771-783.
Nonomura, K., Lukacs, V., Sweet, D.T., Goddard, L.M., Kanie, A., Whitwam, T., Ranade, S.S., Fujimori, T., Kahn, M.L., Patapoutian, A., 2018. Mechanically activated ion channel PIEZO1 is required for lymphatic valve formation. P Natl Acad Sci USA 115, 12817-12822.
Nonomura, K., Woo, S.H., Chang, R.B., Gillich, A., Qiu, Z., Francisco, A.G., Ranade, S.S., Liberles, S.D., Patapoutian, A., 2017. Piezo2 senses airway stretch and mediates lung inflation-induced apnoea. Nature 541, 176-181.
Paix, A., Folkmann, A., Rasoloson, D., Seydoux, G., 2015. High Efficiency, Homology-Directed Genome Editing in Caenorhabditis elegans Using CRISPR-Cas9 Ribonucleoprotein Complexes. Genetics 201, 47-+.
Periasamy, M., Huke, S., 2001. SERCA pump level is a critical determinant of Ca2+ homeostasis and cardiac contractility. J Mol Cell Cardiol 33, 1053-1063.
Poole, K., Herget, R., Lapatsina, L., Ngo, H.D., Lewin, G.R., 2014. Tuning Piezo ion channels to detect molecular-scale movements relevant for fine touch. Nat Commun 5, 3520.
Ranade, S.S., Qiu, Z.Z., Woo, S.H., Hur, S.S., Murthy, S.E., Cahalan, S.M., Xu, J., Mathur, J., Bandell, M., Coste, B., Li, Y.S.J., Chien, S., Patapoutian, A., 2014. Piezo1, a mechanically activated ion channel, is required for vascular development in mice. P Natl Acad Sci USA 111, 10347-10352.
Rual, J.F., Ceron, J., Koreth, J., Hao, T., Nicot, A.S., Hirozane-Kishikawa, T., Vandenhaute, J., Orkin, S.H., Hill, D.E., van den Heuvel, S., Vidal, M., 2004. Toward improving Caenorhabditis elegans phenome mapping with an ORFeome-based RNAi library. Genome Res 14, 2162-2168.
Schindelin, J., Arganda-Carreras, I., Frise, E., Kaynig, V., Longair, M., Pietzsch, T., Preibisch, S., Rueden, C., Saalfeld, S., Schmid, B., Tinevez, J.Y., White, D.J., Hartenstein, V., Eliceiri, K., Tomancak, P., Cardona, A., 2012. Fiji: an open-source platform for biological-image analysis. Nat Methods 9, 676-682.
Singson, A., Mercer, K.B., L'Hernault, S.W., 1998. The C-elegans spe-9 gene encodes a sperm transmembrane protein that contains EGF-like repeats and is required for fertilization. Cell 93, 71-79.
Syeda, R., Xu, J., Dubin, A.E., Coste, B., Mathur, J., Huynh, T., Matzen, J., Lao, J., Tully, D.C., Engels, I.H., Petrassi, H.M., Schumacher, A.M., Montal, M., Bandell, M., Patapoutian, A., 2015. Chemical activation of the mechanotransduction channel Piezo1. Elife 4.
Vicencio, J., Martinez-Fernandez, C., Serrat, X., Ceron, J., 2019. Efficient Generation of Endogenous Fluorescent Reporters by Nested CRISPR in Caenorhabditis elegans. Genetics 211, 1143-1154.
Voglis, G., Tavernarakis, N., 2005. Mechanotransduction in the Nematode Caenorhabditis elegans, in: Kamkin, A., Kiseleva, I. (Eds.), Mechanosensitivity in Cells and Tissues, Moscow.
Whitten, S.J., Miller, M.A., 2007. The role of gap junctions in Caenorhabditis elegans oocyte maturation and fertilization. Developmental Biology 301, 432-446.
Woo, S.H., Lukacs, V., de Nooij, J.C., Zaytseva, D., Criddle, C.R., Francisco, A., Jessell, T.M., Wilkinson, K.A., Patapoutian, A., 2015. Piezo2 is the principal mechanotransduction channel for proprioception. Nat Neurosci 18, 1756-1762.

Woo, S.H., Ranade, S., Weyer, A.D., Dubin, A.E., Baba, Y., Qiu, Z.Z., Petrus, M., Miyamoto, T., Reddy, K., Lumpkin, E.A., Stucky, C.L., Patapoutian, A., 2014. Piezo2 is required for Merkel-cell mechanotransduction. Nature 509, 622-626.

Wu, J., Lewis, A.H., Grandl, J., 2017. Touch, Tension, and Transduction - The Function and Regulation of Piezo Ion Channels. Trends Biochem Sci 42, 57-71.

Yan, X., Xing, J., Lorin-Nebel, C., Estevez, A.Y., Nehrke, K., Lamitina, T., Strange, K., 2006. Function of a STIM1 homologue in C. elegans: evidence that store-operated Ca2+ entry is not essential for oscillatory Ca2+ signaling and ER Ca2+ homeostasis. J Gen Physiol 128, 443-459.

Yang, Y., Han, S.M., Miller, M.A., 2010. MSP hormonal control of the oocyte MAP kinase cascade and reactive oxygen species signaling. Dev Biol 342, 96-107.

Zarychanski, R., Schulz, V.P., Houston, B.L., Maksimova, Y., Houston, D.S., Smith, B., Rinehart, J., Gallagher, P.G., 2012. Mutations in the mechanotransduction protein PIEZO1 are associated with hereditary xerocytosis. Blood 120, 1908-1915.

Zhang, L., Ward, J.D., Cheng, Z., Dernburg, A.F., 2015. The auxin-inducible degradation (AID) system enables versatile conditional protein depletion in C. elegans. Development 142, 4374-4384.

Zhang, M., Wang, Y., Geng, J., Zhou, S., Xiao, B., 2019. Mechanically Activated Piezo Channels Mediate Touch and Suppress Acute Mechanical Pain Response in Mice. Cell Rep 26, 1419-1431 e1414.

Zhang, T., Chi, S., Jiang, F., Zhao, Q., Xiao, B., 2017. A protein interaction mechanism for suppressing the mechanosensitive Piezo channels. Nat Commun 8, 1797.

Zwaal, R.R., Van Baelen, K., Groenen, J.T.M., van Geel, A., Rottiers, V., Kaletta, T., Dode, L., Raeymaekers, L., Wuytack, F., Bogaert, T., 2001. The sarco-endoplasmic reticulum Ca2+ ATPase is required for development and muscle function in Caenorhabditis elegans. J Biol Chem 276, 43557-43563.

1478 **Table 1 *C. elegans* strains list in the study.**

1479

	Strain	Genotype
Fig.1	AG404	*pezo-1(av142[mScarlet::pezo-1]) IV. CRISPR/Cas9 Edit*
	AG408	*pezo-1(av146 [gfp::pezo-1]) IV. CRISPR/Cas9 Edit*
	AG483	*pezo-1(av182 [pezo-1::mScarlet]) IV. CRISPR/Cas9 Edit*
Fig.2	N2	Bristol (wild-type)
	AG406	*pezo-1(av144[N-Δ]) IV. CRISPR/Cas9 Edit. Deletion of exon 1-13 and introns*
	AG416	*pezo-1(av149[C-Δ]) IV. CRISPR/Cas9 Edit. Deletion of exon 27-33 and introns*
	AG530	*pezo-1(av149[C-Δ]) IV; ruIs32 [pie-1p::GFP::H2B + unc-119(+)] III.*
	AZ212	*ruIs32 [pie-1p::GFP::H2B + unc-119(+)] III.*
Fig.3	N2	Bristol (wild-type)
	AG416	*pezo-1(av149) IV. CRISPR/Cas9 Edit. Deletion of exon 27-33 and introns*
	LP598	*dlg-1(cp301[dlg-1::mNG-C1^3xFlag]) X. CRISPR/Cas9 Edit*
	AG491	*pezo-1(av149) IV; dlg-1(cp301[dlg-1::mNG-C1^3xFlag]) X.*
Fig.4	N2	Bristol (wild-type)
	AG416	*pezo-1(av149) IV. CRISPR/Cas9 Edit. Deletion of exon 27-33 and introns*
Fig. 5	UN1108	*xbIs1101 [fln-1p::GCaMP3; pRF4(rol-6^{D}(su1006))] II*
	AG414	*pezo-1(av144)* IV*; xbIs1101 [fln-1p::GCaMP3; pRF4(rol-6^{D}(su1006))] II*
	AG415	*pezo-1(av149)* IV*; xbIs1101 [fln-1p::GCaMP3; pRF4(rol-6^{D}(su1006))] II*
	AG448	*pezo-1(av142 [mScarlet::pezo-1]) IV; xbIs1101 [fln-1p::GCaMP3; pRF4(rol-6^{D}(su1006))] II*
Fig.6	N2	Bristol (wild-type)
	AG406	*pezo-1(av144) IV. CRISPR/Cas9 Edit. Deletion of exon 1-13 and introns*
	AG416	*pezo-1(av149) IV. CRISPR/Cas9 Edit. Deletion of exon 27-33 and introns*
	AG531	*spe-9(hc52ts) I; him-8(e1489) IV*
	BA17	*fem-1(hc17ts) IV*
	CB1489	*him-8(e1489) IV*
Fig.7	N2	Bristol (wild-type)
	AG416	*pezo-1(av149) IV. CRISPR/Cas9 Edit. Deletion of exon 27-33 and introns*
Fig.8	N2	Bristol (wild-type)
	AG487	*pezo-1(av190 [pezo-1::degron]) IV. CRISPR/Cas9 Edit.*
	AG493	*pezo-1(av190 [pezo-1::degron]) IV; ieSi65 [sun-1p::TIR1::sun-1 3'UTR + Cbr-unc-119(+)] II; unc-119(ed3) III.*
	AG494	*pezo-1(av190 [pezo-1::degron]) IV; ieSi57 [eft-3p::TIR1::mRuby::unc-54 3'UTR + Cbr-unc-119(+)] II*
	AG495	*pezo-1(av190[pezo-1::degron]) IV; fxIs1[pie-1p::TIR1::mRuby] I*
	AG564	*fxIs1[pie-1p::TIR1::mRuby] I*
	AG565	*ieSi65 [sun-1p::TIR1::sun-1 3'UTR + Cbr-unc-119(+)] II; unc-119(ed3) III.*
	AG566	*ieSi57 [eft-3p::TIR1::mRuby::unc-54 3'UTR + Cbr-unc-119(+)] II*
Fig.9	N2	Bristol (wild-type)
	AG437	*pezo-1(av165[R2405P]) IV. CRISPR/Cas9 Edit.*
	AG531	*spe-9(hc52ts) I; him-8(e1489) IV*
Fig.S1	AG404	*pezo-1(av142 [mScarlet::pezo-1]) IV. CRISPR/Cas9 Edit*

	AG408	*pezo-1(av146 [gfp::pezo-1]) IV. CRISPR/Cas9 Edit*
	AG483	*pezo-1(av182 [pezo-1::mScarlet]) IV. CRISPR/Cas9 Edit*
Fig.S2	N2	Bristol (wild-type)
	AG406	*pezo-1(av144) IV. CRISPR/Cas9 Edit. Deletion of exon 1-13 and introns*
	AG416	*pezo-1(av149) IV. CRISPR/Cas9 Edit. Deletion of exon 27-33 and introns*
	PS8111	*pezo-1(sy1199) IV. CRISPR/Cas9 Edit. CRISPR/Cas9 Edit. Stop-cassette*
	PS8546	*pezo-1(sy1398) IV. CRISPR/Cas9 Edit. Deletion of the first exon of isoforms i and j*
	AG570	*pezo-1(av240) IV. CRISPR/Cas9 Edit. Deletion of full length of pezo-1.*
Fig.S3	UN1108	*xbIs1101 [fln-1p::GCaMP3; pRF4(rol-6^{D}(su1006))] II*
	AG414	*pezo-1(av144) IV; xbIs1101 [fln-1p::GCaMP3; pRF4(rol-6^{D}(su1006))] II*
	AG415	*pezo-1(av149) IV; xbIs1101 [fln-1p::GCaMP3; pRF4(rol-6^{D}(su1006))] II*
Fig.S4	AG494	*pezo-1(av190 [pezo-1::degron]) IV; ieSi57 [eft-3p::TIR1::mRuby::unc-54 3'UTR + Cbr-unc-119(+)] II*
	AG416	*pezo-1(av149) IV. CRISPR/Cas9 Edit. Deletion of exon 27-33 and introns*
	BA17	*fem-1(hc17ts) IV*
	AG571	*pezo-1(av149) IV; fem-1(hc17ts) IV*
Fig.S5	AG493	*pezo-1(av190 [pezo-1::degron]) IV; ieSi65 [sun-1p::TIR1::sun-1 3'UTR + Cbr-unc-119(+)] II; unc-119(ed3) III.*
	AG494	*pezo-1(av190 [pezo-1::degron]) IV; ieSi57 [eft-3p::TIR1::mRuby::unc-54 3'UTR + Cbr-unc-119(+)] II*
	AG495	*pezo-1(av190[pezo-1::degron]) IV; fxIs1[pie-1p::TIR1::mRuby] I*
Fig.S6	AG582	*pezo-1(av241 [gfp::pezo-1::degron]) IV. CRISPR/Cas9 Edit*
	AG567	*pezo-1(av241 [gfp::pezo-1::degron]) IV; ieSi57 [eft-3p::TIR1::mRuby::unc-54 3'UTR + Cbr-unc-119(+)] II*
	AG568	*pezo-1(av241 [gfp::pezo-1::degron]) IV; fxIs1[pie-1p::TIR1::mRuby] I*
	AG569	*pezo-1(av241 [gfp::pezo-1::degron]) IV; ieSi65 [sun-1p::TIR1::sun-1 3'UTR + Cbr-unc-119(+)] II; unc-119(ed3) III.*
Fig.S7	AG494	*pezo-1(av190 [pezo-1::degron]) IV; ieSi57 [eft-3p::TIR1::mRuby::unc-54 3'UTR + Cbr-unc-119(+)] II*
Video.S1	AG408	*pezo-1(av146 [gfp::pezo-1]) IV. CRISPR/Cas9 Edit*
Video.S2	N2	Bristol (wild-type)
	AG406	*pezo-1(av149)] IV. CRISPR/Cas9 Edit. Deletion of exon 27-33 and introns*
Video.S3	LP598	*dlg-1(cp301[dlg-1::mNG-C1^3xFlag]) X. CRISPR/Cas9 Edit*
	AG491	*pezo-1(av149) IV; dlg-1(cp301[dlg-1::mNG-C1^3xFlag]) X.*
Video.S4	AG406	*pezo-1(av149) IV. CRISPR/Cas9 Edit. Deletion of exon 27-33 and introns*
Video.S5	AG448	*pezo-1(av142 [mScarlet::pezo-1]) IV; xbIs1101 [fln-1p::GCaMP3; pRF4(rol-6^{D}(su1006))] II*
Video.S6	UN1108	*xbIs1101 [fln-1p::GCaMP3; pRF4(rol-6^{D}(su1006))] II*
	AG415	*pezo-1(av149) IV; xbIs1101 [fln-1p::GCaMP3; pRF4(rol-6^{D}(su1006))] II*

Table 2 List of the sequence for the CRISPR design

Strain	Genotype	Description	Sequence Name	Sequence 5'-3'	PAM
AG406	*pezo-1 (av144)* IV.	Deletion of exons 1-13 and introns of *pezo-1*	crRNA N-terminus	ACACAGCAACAACAGAATGA	CGG
			crRNA C-terminus	TGGGGGTGTTGCAGTGGCTA	AGG
			Repair Template	atctgaatcggtggtcgtaacacagcaacaacaga**g**tttgacacattttccgttgagacttgaaaaatag	
			Genotyping F1	GCGGTAAATCTGAATCGGTGG	
			Genotyping R1	TTGGAAAAGCAGGCACAACC	
			Genotyping Internal	CGATCCAGCGTGGATGAACT	
AG416	*pezo-1 (av149)* IV.	Deletion of exons 27-33 and introns of *pezo-1*	crRNA N-terminus	CGGTGGCAGCGTACATTATC	TGG
			crRNA C-terminus	CACCAGCGACACTCATCGAA	TGG
			Repair Template	tccagtctcccatatttatttttttctgttccagT**A**G**T**A**A**G**T**A**A**GAGCAAAAAGAAGCAAGAATAA	
			Genotyping F1	AATCTGACTTGTGCCCTCCG	
			Genotyping R1	AATCAGGCGAGCAGTGAGAG	
			Genotyping Internal	TCCACAGTCAATTCCTGCGT	
AG404	*pezo-1(av142 [mScarlet::pezo-1])* IV	Knock in mScarlet at N-terminus of *pezo-1, mScarlet* was amplified from plasmid pMS050	crRNA	ACACAGCAACAACAGAATGA	CGG
			Repair Template F1	tgaatcggtggtcgtaacacagcaacaacagaATG CTTGTAGAGCTCGTCCATTCC (mScarlet)	
			Repair Template R1	AATTTGACGACGCACGATTTTAAAAGCGGCGGGAC**T**GT CTTGTAGAGCTCGTCCATTCC (mScarlet)	
AG408	*pezo-1(av146 [gfp::pezo-1])* IV.	Knock in GFP at N-terminus of *pezo-1,* GFP was amplified from plasmid pDD282	crRNA	ACACAGCAACAACAGAATGA	CGG
			Repair Template F1	tgaatcggtggtcgtaacacagcaacaacagaATG agtaaaggagaagaattgttc (GFP)	
			Repair Template R1	AATTTGACGACGCACGATTTTAAAAGCGGCGGGAC**T**GT CTTGTAGAGCTCGTCCATTC (GFP)	
AG483	*pezo-1(av182 [pezo-1::mScarlet])* IV.	Knock in mScarlet at C-terminus of *pezo-1,* mScarlet was amplified from plasmid pMS050	NEST1 crRNA	CACCAGCGACACTCATCGAA	TGG
			Repair Template	AATATTCCTGTTCCGATCACCAGCGACACTCATCGAA**TGG**AC**T**CG**T**ATGAG**T**AA**G**AA**A**A A**A**CA**G**GA**G** GTCTCCAAGGGAGAGGCCGTCATCAAGGAGTTCATGCGTTTCAAGGTCCAAGCG**C**TCC GAGGGACGTCACT**CCA**CCGGAGGAATGGACGAGCTCTACAAGTAAatttaaatatttcactgtca aatattctgcga (mScarlet)	
			Genotyping F1	TGGTTCGAGAAGCGAAGGAC	
			Genotyping R1	aatcaggcgagcagtgagag	

			NEST2 crRNA	TTCAAGGTCCAAGCG**C**TCCG	AGG
			Repair Template F1	GCCGTCATCAAGGAGTTCATGCGTTTCAAGGTCCACATGGAGGGATCCATGAACG	
			Repair Template R1	TAGAGCTCGTCCATTCCTCCGGTGGAGTGACGTCC**T**TC**T**GA**A**CGCTCGTATTGCTCGA CGACGGTG	
AG487	*pezo-1(av190 [pezo-1::degron])* IV	Knock in Degron sequence at C-terminus of *pezo-1.* Degron was amplified from plasmid pK0132	crRNA	CACCAGCGACACTCATCGAA	TGG
			Repair Template F1	AATATTCCTGTTCCGATCACCAGCGACACTCATCGAA**TGG**AC**T**CG**T**ATGAG**T**A A**G**AA**A**AA**A**CA**G**GA**G**ggagcatcgggagcctcaggagcatcg(linker)GACTACAAAGACCA TGACGGTG (Degron)	
			Repair Template R1	tcgcagaatatttgacagtgaaatatttaaatTTACTTCACGAACGCCGCC(Degron)	
AG437	*pezo-1(av165*[R2405P]*)* IV	Generate a point mutation R2405P in *pezo-1*	crRNA	CTATTTGGTTCGAGAAGCGA	AGG
			Repair Template	CATCTTCTCAAAATTTGTCTCGACATCTATTTGGTACCAGAAGCGAAAGACTTC ATGTTGGAGCAGgtaattatttagtttta	
AG570	*pezo-1(av240)* IV.	Deletion of full length of *pezo-1*	crRNA1	ACACAGCAACAACAGAATGA	CGG
			crRNA2	CACCAGCGACACTCATCGAA	TGG
			Repair Template	ctgaatcggtggtcgtaacacagcaacaacagaATGT**A**GATAAGTAAGAGCAAAAAGAAGCA AGAATAAatttaaatatttc	
AG571	*pezo-1(av242)* IV.	Deletion of exons 27-33 and introns of *pezo-1 in fem-1(hc17)*	crRNA1	CGGTGGCAGCGTACATTATC	TGG
			crRNA2	CACCAGCGACACTCATCGAA	TGG
			Repair Template	tccagtctcccatatttatttttttctgttccagT**A**GA**T**A**A**G**T**A**A**GAGCAAAAAGAAGCAAGAATAA	
AG582	*pezo-1(av241)* IV.	Knock in Degron sequence at C-terminus of *pezo-1* in AG404. Degron was amplified from plasmid pK0132	crRNA	CACCAGCGACACTCATCGAA	TGG
			Repair Template F1	AATATTCCTGTTCCGATCACCAGCGACACTCATCGAA**TGG**AC**T**CG**T**ATGAG**T**A A**G**AA**A**AA**A**CA**G**GA**G**ggagcatcgggagcctcaggagcatcg(linker)GACTACAAAGACCA TGACGGTG (Degron)	
			Repair Template R1	tcgcagaatatttgacagtgaaatatttaaatTTACTTCACGAACGCCGCC(Degron)	
PS8111	*pezo-1(sy1199)* IV	Knock in a stop cassette at C-terminus of *pezo-1*	crRNA	CCAGAAGCTCGTAAGCCAGG	AGG
			Repair Template	cttatcgctgtttctgaaccagaagctcgtaagccGGGAAGTTTGTCCAGAGCAGAGGTGACTA AGTGATAAgctagcaggaggcactgaagaaacggatggtgatgaag	
			Genotyping F1	GACAGGACTTTCCCGCCAACTTAA	
			Genotyping R1	ATCATTCGCCGATTGCACAAGTTG	
PS8546	*pezo-1(sy1398)* IV	Deletion of the first exon of *pezo-1* isoforms i	crRNA1	gagaacttgaattcaatgg	AGG
			crRNA2	aagcttcttccgtctccgg	CGG
			crRNA3	gcagtatttgaccaactgg	TGG

		and j	crRNA4	ataaaacaaggcaaccagg	GGG
			Genotyping F1	CTCTCGCCTATCCACTTGAGCTTA	
			Genotyping R1	GGAAACAATTGAGCCGAGAATGGA	

Note: Capital letters represent the ORF or exon sequence, small letters indicate the sequence from intron. Bolded letters indicate the optimized base needed for the CRISPR design.

Figure 1

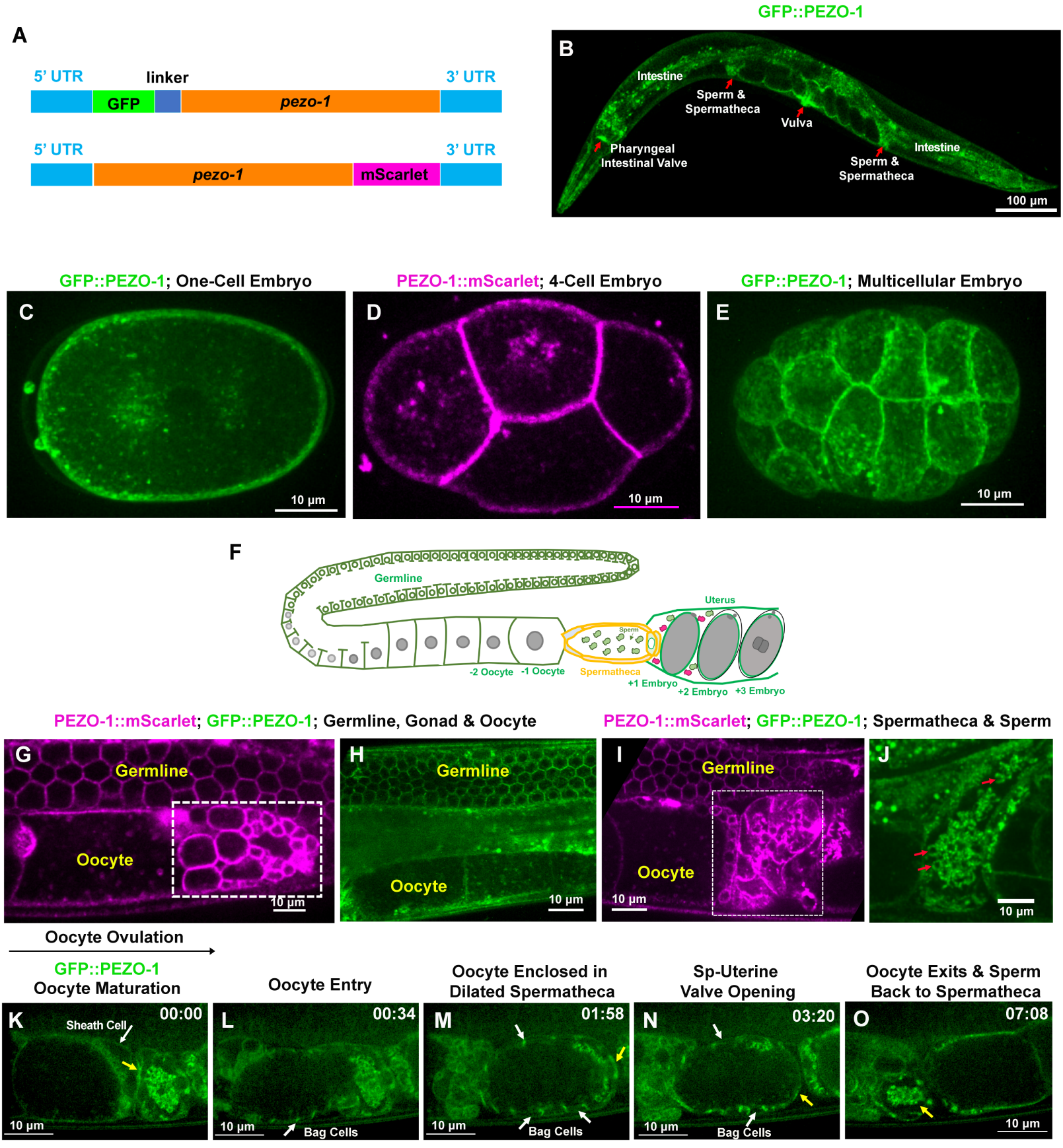
A
5' UTR
linker
3' UTR
GFP
pezo-1
5' UTR
3' UTR
pezo-1
mScarlet
GFP::PEZO-1
B
Intestine
Sperm & Spermatheca
Vulva
Pharyngeal Intestinal Valve
Intestine
Sperm & Spermatheca
100 µm
GFP::PEZO-1; One-Cell Embryo
PEZO-1::mScarlet; 4-Cell Embryo
GFP::PEZO-1; Multicellular Embryo
C
10 µm
D
10 µm
E
10 µm
F
Germline
Uterus
Sperm
-2 Oocyte
-1 Oocyte
Spermatheca
+1 Embryo
+2 Embryo
+3 Embryo
PEZO-1::mScarlet; GFP::PEZO-1; Germline, Gonad & Oocyte
PEZO-1::mScarlet; GFP::PEZO-1; Spermatheca & Sperm
G
Germline
Oocyte
10 µm
H
Germline
Oocyte
10 µm
I
Germline
Oocyte
10 µm
J
10 µm
Oocyte Ovulation
GFP::PEZO-1
Oocyte Maturation
Oocyte Entry
Oocyte Enclosed in Dilated Spermatheca
Sp-Uterine Valve Opening
Oocyte Exits & Sperm Back to Spermatheca
K
Sheath Cell
00:00
10 µm
L
00:34
10 µm
Bag Cells
M
01:58
10 µm
Bag Cells
N
03:20
10 µm
Bag Cells
O
07:08
10 µm

Figure 1- figure supplement 1

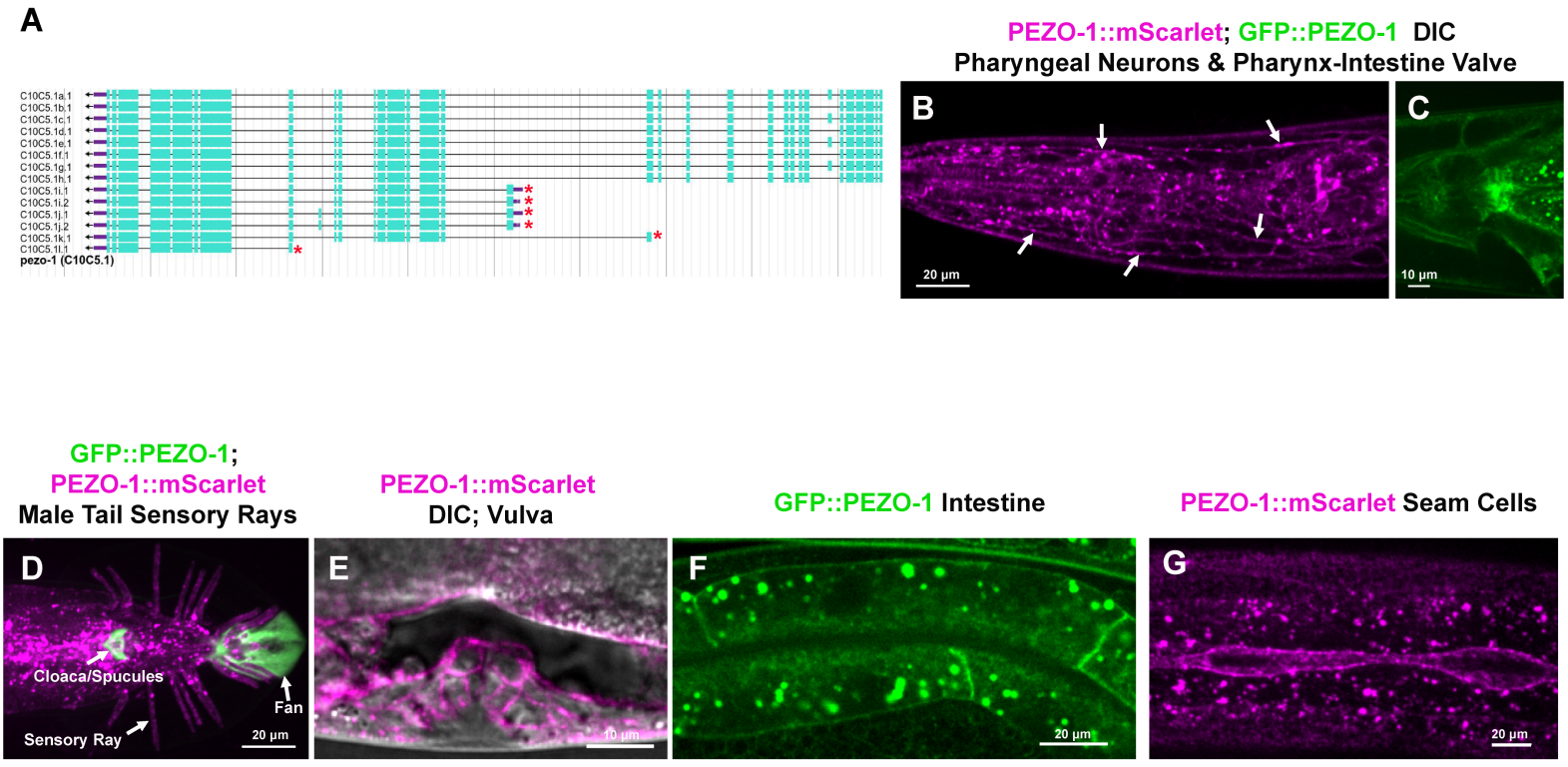

Figure 2

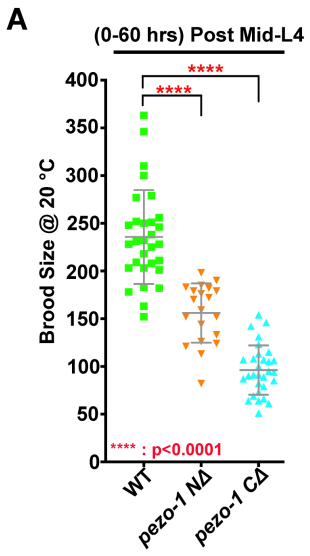

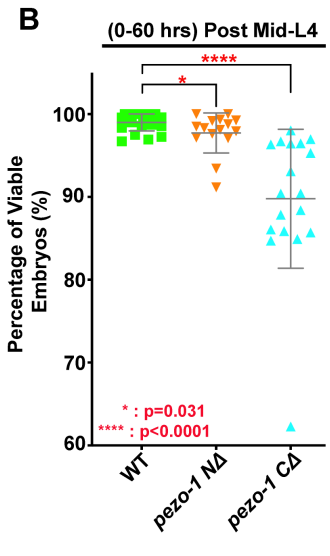

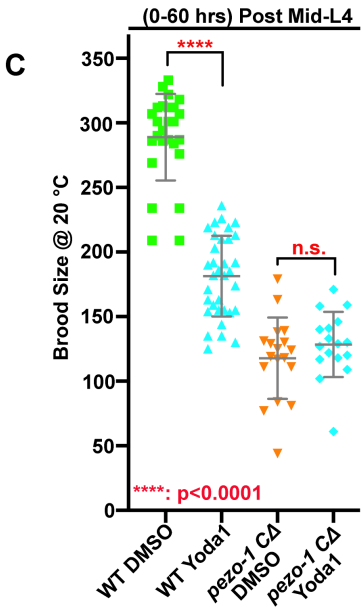

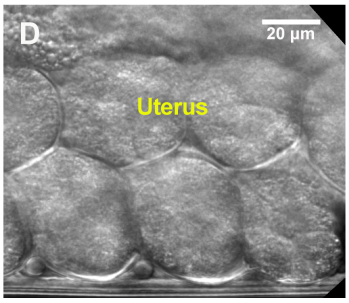

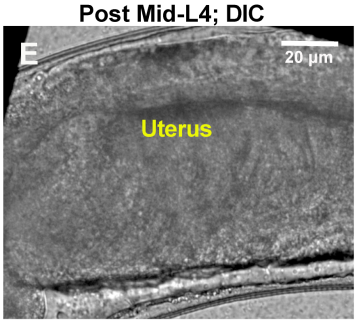

F

Genotype	# Hours Post-L4	Uteri with Ooplasmic Masses
N2	36 hours	0% (0/22)
	48 hours	0% (0/35)
	60 hours	0% (0/15)
pezo-1 NΔ	36 hours	28.0% (7/25)
	48 hours	28.9% (17/59)
	60 hours	20.0% (3/15)
pezo-1 CΔ	36 hours	65.2% (15/23)
	48 hours	79.2% (42/53)
	60 hours	100% (15/15)

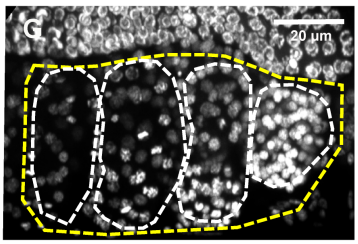

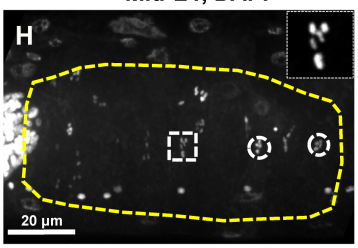

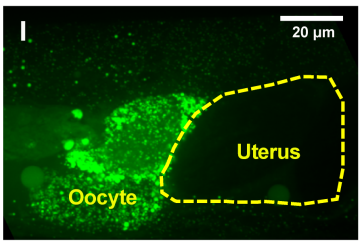

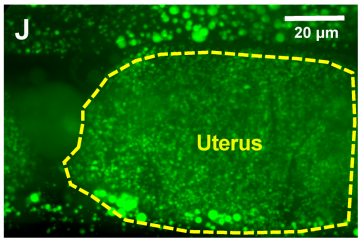

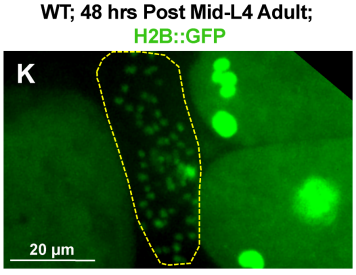

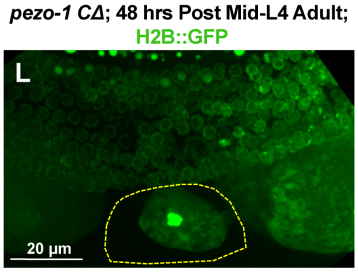

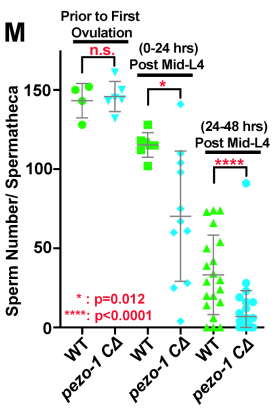

N

Genotype	# Hours Post Mid-L4	# Ovulations per hour	# Tested Gonad Arms
Wild Type	24 hours	2.29 ± 0.92	17
Wild Type	48 hours	1.72 ± 1.10	25
pezo-1 CΔ	24 hours	1.36 ± 0.74	33
pezo-1 CΔ	48 hours	0.25 ± 0.44	20

Figure 2- figure supplement 1

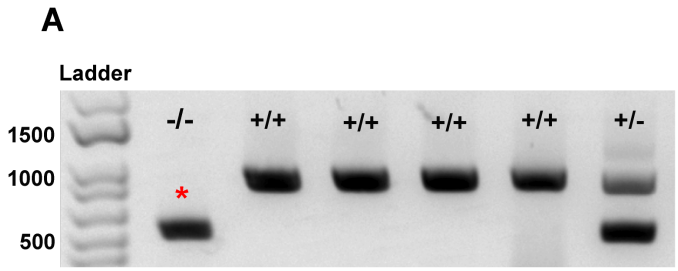

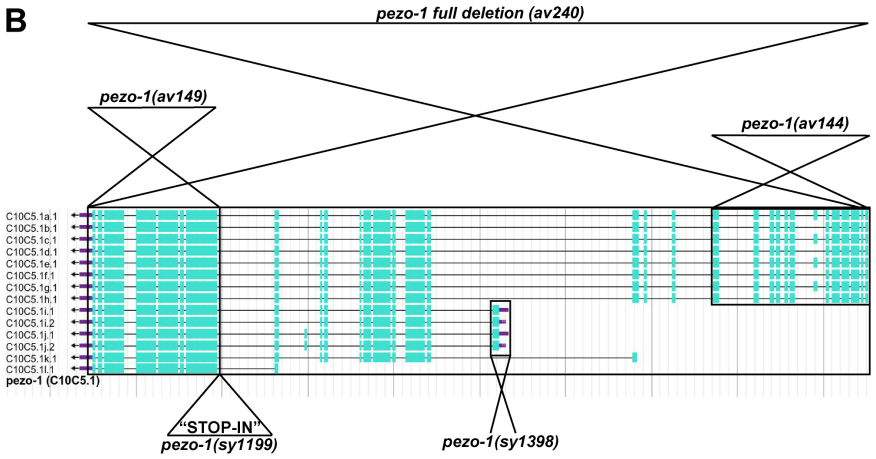

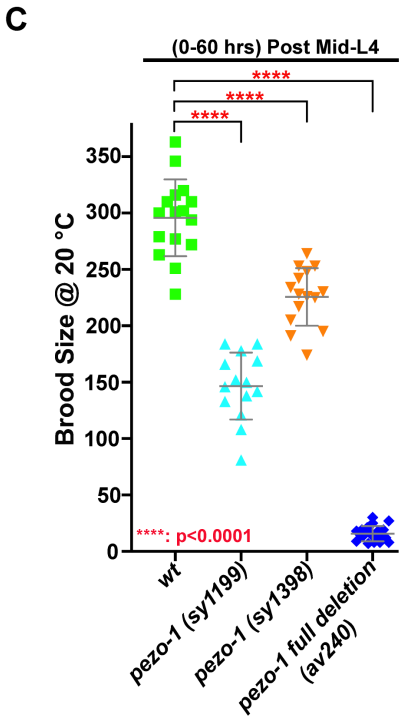

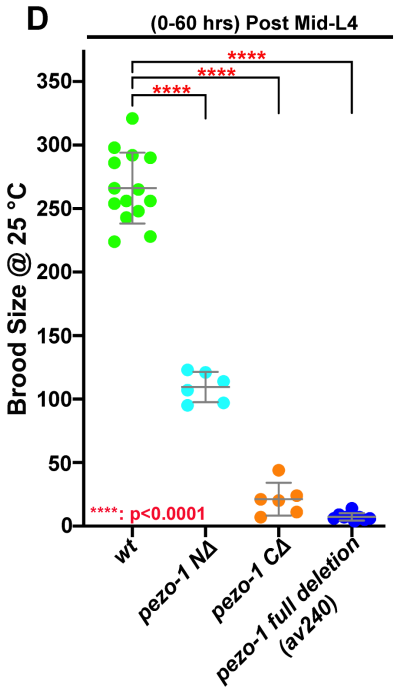

E

Genotype	# of hrs Post Mid-L4	Uteri with Ooplasmic Mass
pezo-1 (sy1199)	36 hours	50.0% (7/14)
	60 hours	100% (14/14)
pezo-1 (sy1398)	36 hours	6.7% (1/15)
	60 hours	26.7% (4/15)

Figure 3

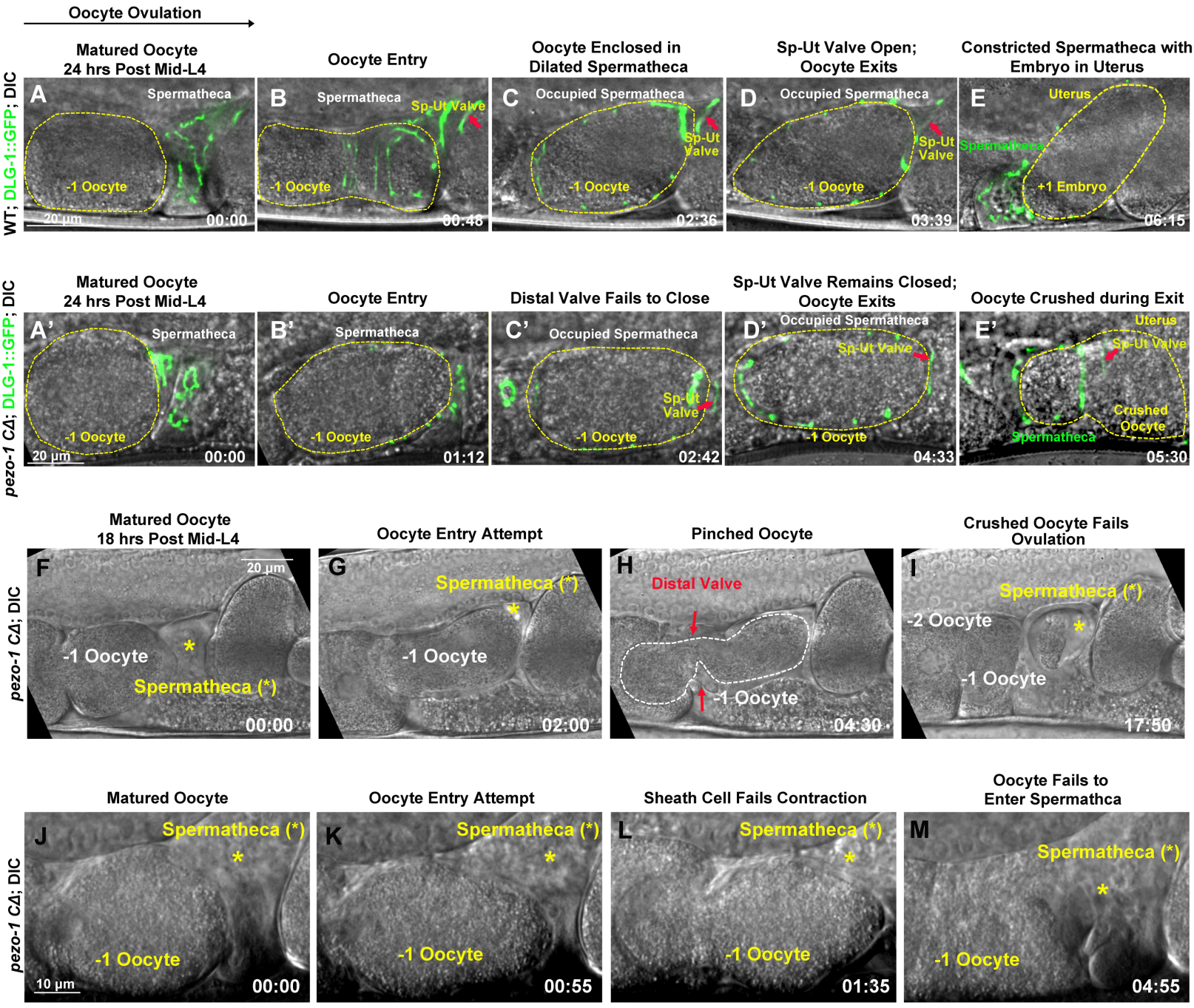
Oocyte Ovulation
WT; DLG-1::GFP; DIC
Matured Oocyte
24 hrs Post Mid-L4
Oocyte Entry
Oocyte Enclosed in
Dilated Spermatheca
Sp-Ut Valve Open;
Oocyte Exits
Constricted Spermatheca with
Embryo in Uterus
A
Spermatheca
-1 Oocyte
20 µm
00:00
B
Spermatheca
Sp-Ut Valve
-1 Oocyte
00:48
C
Occupied Spermatheca
Sp-Ut Valve
-1 Oocyte
02:36
D
Occupied Spermatheca
Sp-Ut Valve
-1 Oocyte
03:39
E
Uterus
Spermatheca
+1 Embryo
06:15
pezo-1 CΔ; DLG-1::GFP; DIC
Matured Oocyte
24 hrs Post Mid-L4
Oocyte Entry
Distal Valve Fails to Close
Sp-Ut Valve Remains Closed;
Oocyte Exits
Oocyte Crushed during Exit
A'
Spermatheca
-1 Oocyte
20 µm
00:00
B'
Spermatheca
-1 Oocyte
01:12
C'
Occupied Spermatheca
Sp-Ut Valve
-1 Oocyte
02:42
D'
Occupied Spermatheca
Sp-Ut Valve
-1 Oocyte
04:33
E'
Uterus
Sp-Ut Valve
Crushed Oocyte
Spermatheca
05:30
pezo-1 CΔ; DIC
Matured Oocyte
18 hrs Post Mid-L4
Oocyte Entry Attempt
Pinched Oocyte
Crushed Oocyte Fails
Ovulation
F
20 µm
-1 Oocyte
Spermatheca (*)
00:00
G
Spermatheca (*)
-1 Oocyte
02:00
H
Distal Valve
-1 Oocyte
04:30
I
Spermatheca (*)
-2 Oocyte
-1 Oocyte
17:50
pezo-1 CΔ; DIC
Matured Oocyte
Oocyte Entry Attempt
Sheath Cell Fails Contraction
Oocyte Fails to
Enter Spermathca
J
Spermatheca (*)
-1 Oocyte
10 µm
00:00
K
Spermatheca (*)
-1 Oocyte
00:55
L
Spermatheca (*)
-1 Oocyte
01:35
M
Spermatheca (*)
-1 Oocyte
04:55

Figure 4

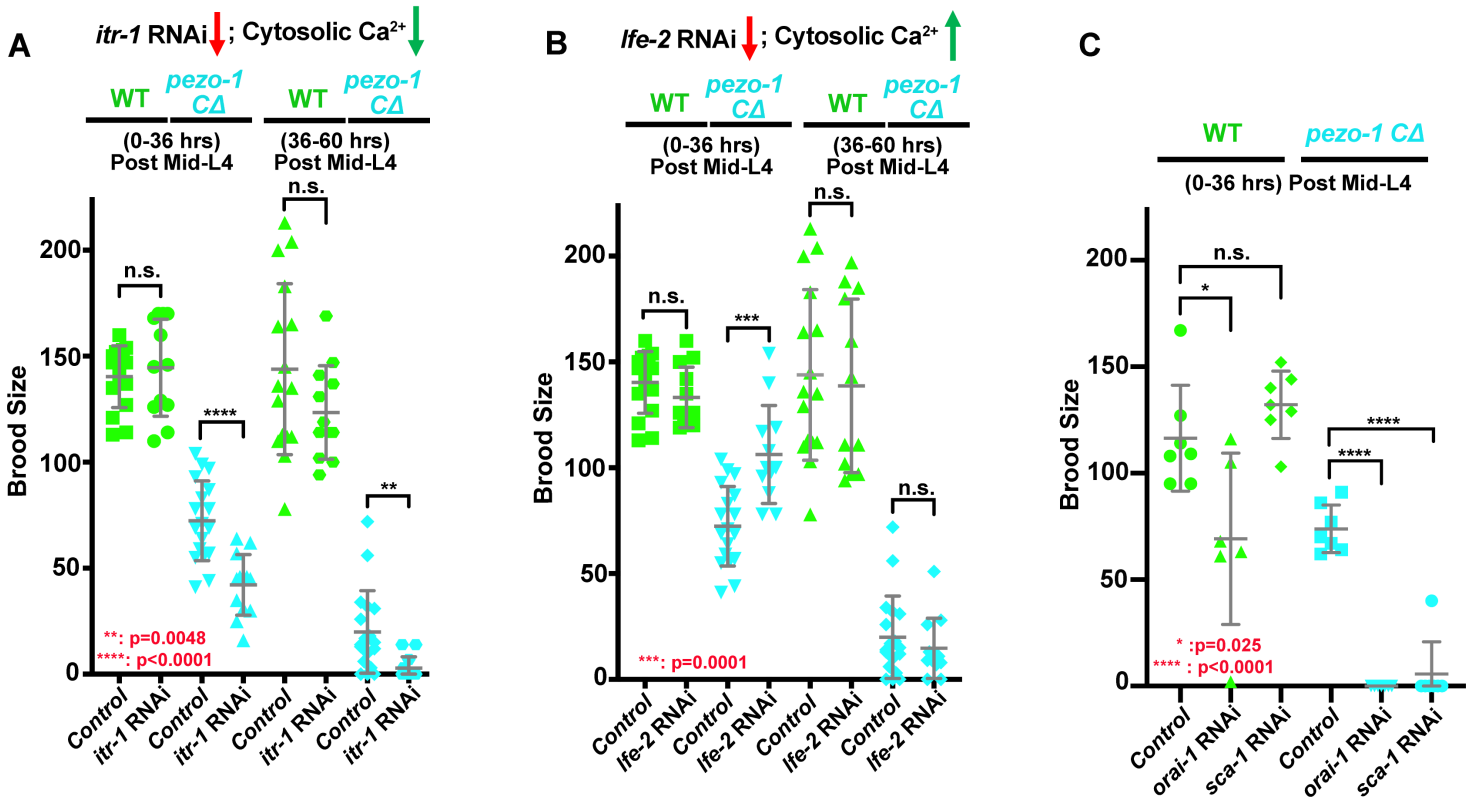
A
itr-1 RNAi ↓; Cytosolic Ca2+ ↓
WT
pezo-1 CΔ
WT
pezo-1 CΔ
(0-36 hrs) Post Mid-L4
(36-60 hrs) Post Mid-L4
Brood Size
n.s.
****
n.s.
**
**: p=0.0048
****: p<0.0001
Control
itr-1 RNAi
Control
itr-1 RNAi
Control
itr-1 RNAi
Control
itr-1 RNAi
B
lfe-2 RNAi ↓; Cytosolic Ca2+ ↑
WT
pezo-1 CΔ
WT
pezo-1 CΔ
(0-36 hrs) Post Mid-L4
(36-60 hrs) Post Mid-L4
Brood Size
n.s.
***
n.s.
n.s.
***: p=0.0001
Control
lfe-2 RNAi
Control
lfe-2 RNAi
Control
lfe-2 RNAi
Control
lfe-2 RNAi
C
WT
pezo-1 CΔ
(0-36 hrs) Post Mid-L4
Brood Size
n.s.
*
****
****
* :p=0.025
**** : p<0.0001
Control
orai-1 RNAi
sca-1 RNAi
Control
orai-1 RNAi
sca-1 RNAi

Figure 5

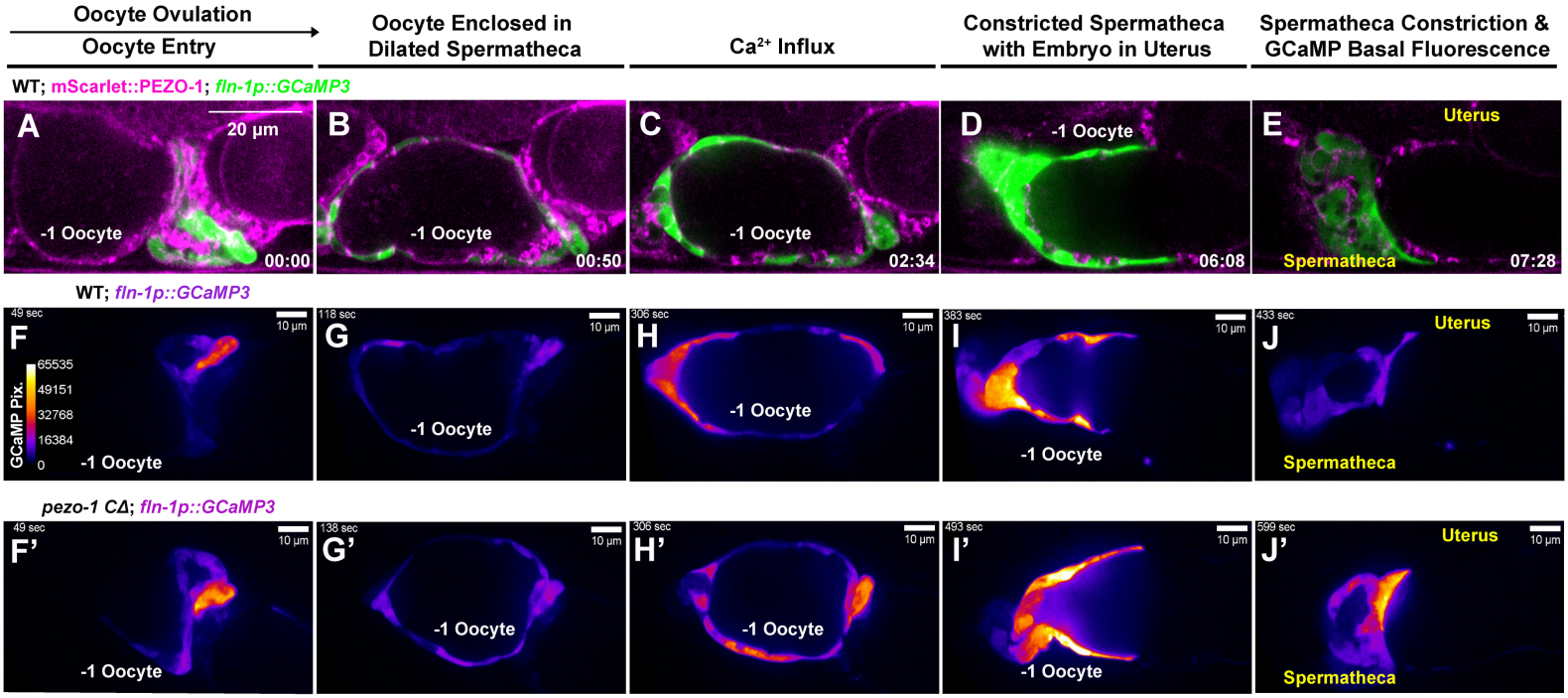
Oocyte Ovulation
Oocyte Entry
Oocyte Enclosed in Dilated Spermatheca
Ca2+ Influx
Constricted Spermatheca with Embryo in Uterus
Spermatheca Constriction & GCaMP Basal Fluorescence
WT; mScarlet::PEZO-1; fln-1p::GCaMP3
A
20 µm
-1 Oocyte
00:00
B
-1 Oocyte
00:50
C
-1 Oocyte
02:34
D
-1 Oocyte
06:08
E
Uterus
Spermatheca
07:28
WT; fln-1p::GCaMP3
F
49 sec
10 µm
GCaMP Pix.
65535
49151
32768
16384
0
-1 Oocyte
G
118 sec
10 µm
-1 Oocyte
H
306 sec
10 µm
-1 Oocyte
I
383 sec
10 µm
-1 Oocyte
J
433 sec
10 µm
Uterus
Spermatheca
pezo-1 CΔ; fln-1p::GCaMP3
F'
49 sec
10 µm
-1 Oocyte
G'
138 sec
10 µm
-1 Oocyte
H'
306 sec
10 µm
-1 Oocyte
I'
493 sec
10 µm
-1 Oocyte
J'
599 sec
10 µm
Uterus
Spermatheca

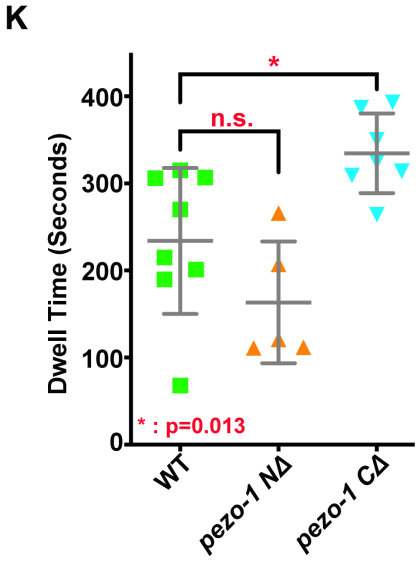
K
Dwell Time (Seconds)
400
300
200
100
0
*
n.s.
* : p=0.013
WT
pezo-1 NΔ
pezo-1 CΔ

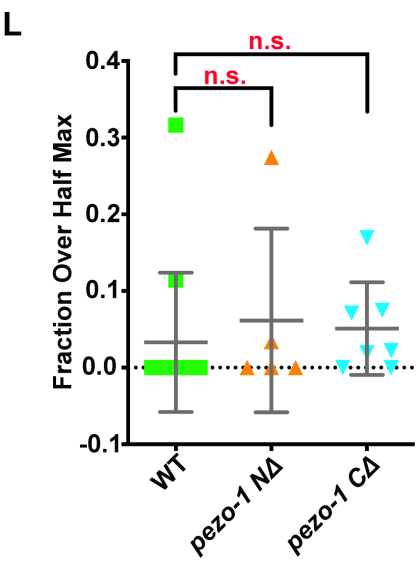
L
Fraction Over Half Max
0.4
0.3
0.2
0.1
0.0
-0.1
n.s.
n.s.
WT
pezo-1 NΔ
pezo-1 CΔ

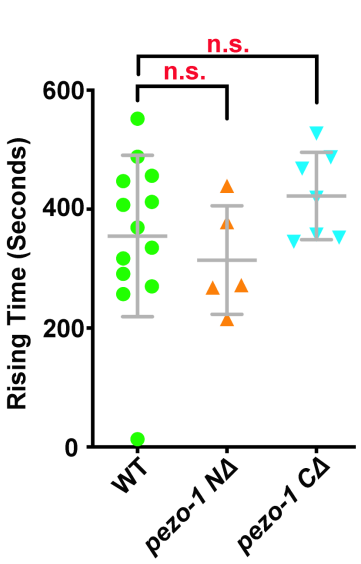
M
Rising Time (Seconds)
600
400
200
0
n.s.
n.s.
WT
pezo-1 NΔ
pezo-1 CΔ

Figure 5- figure supplement 1

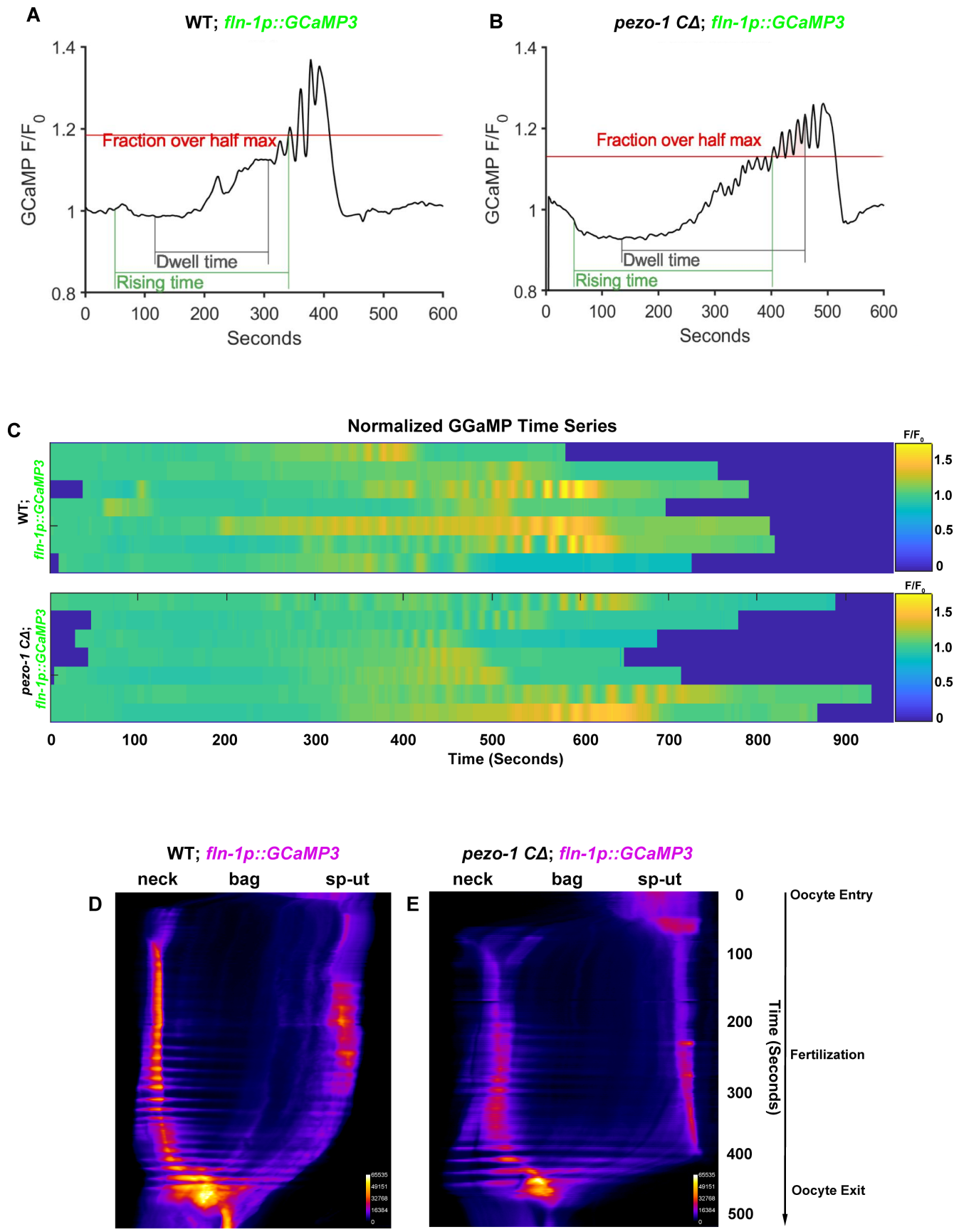

Figure 6-figure supplement 1

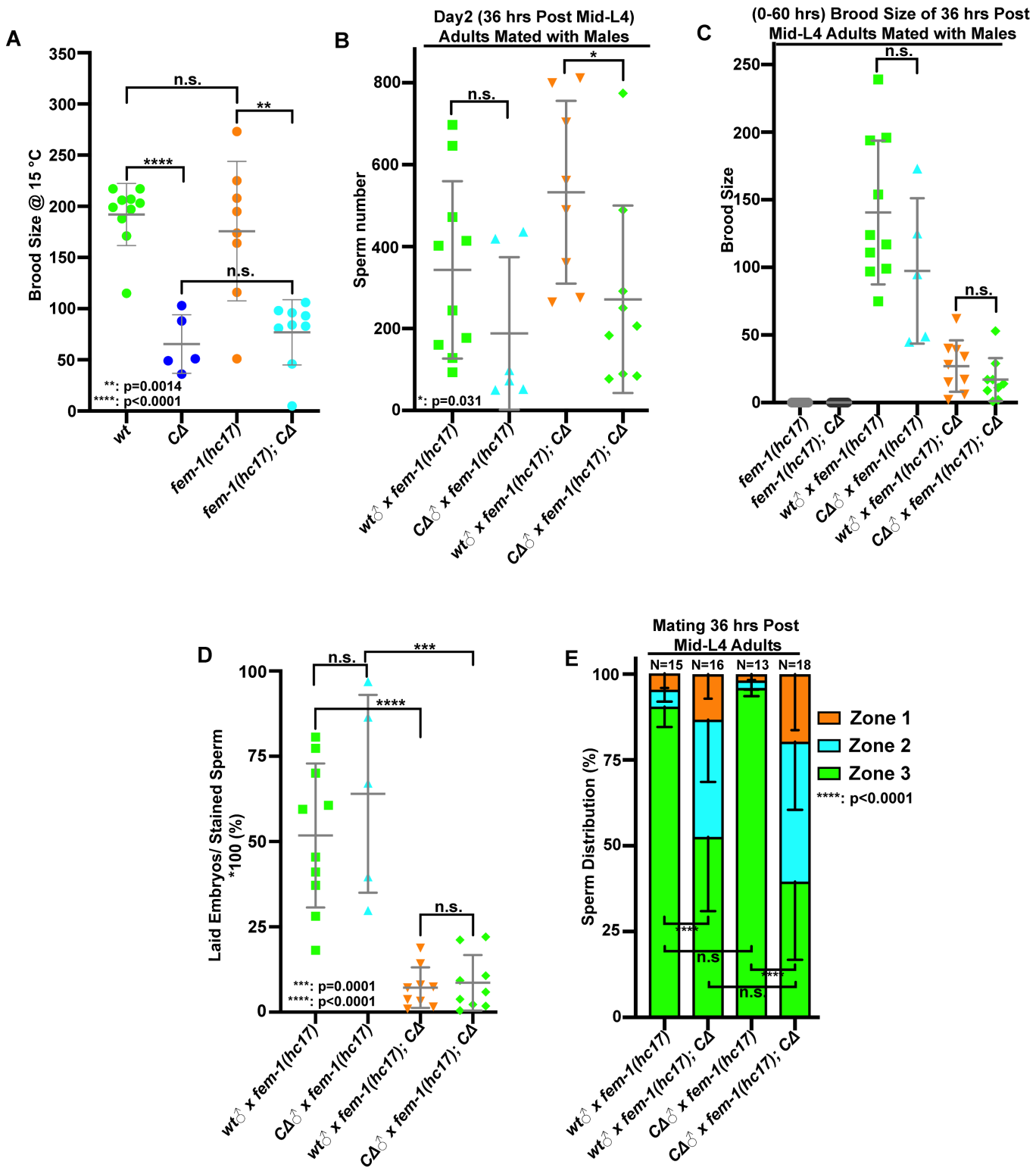

Figure 7

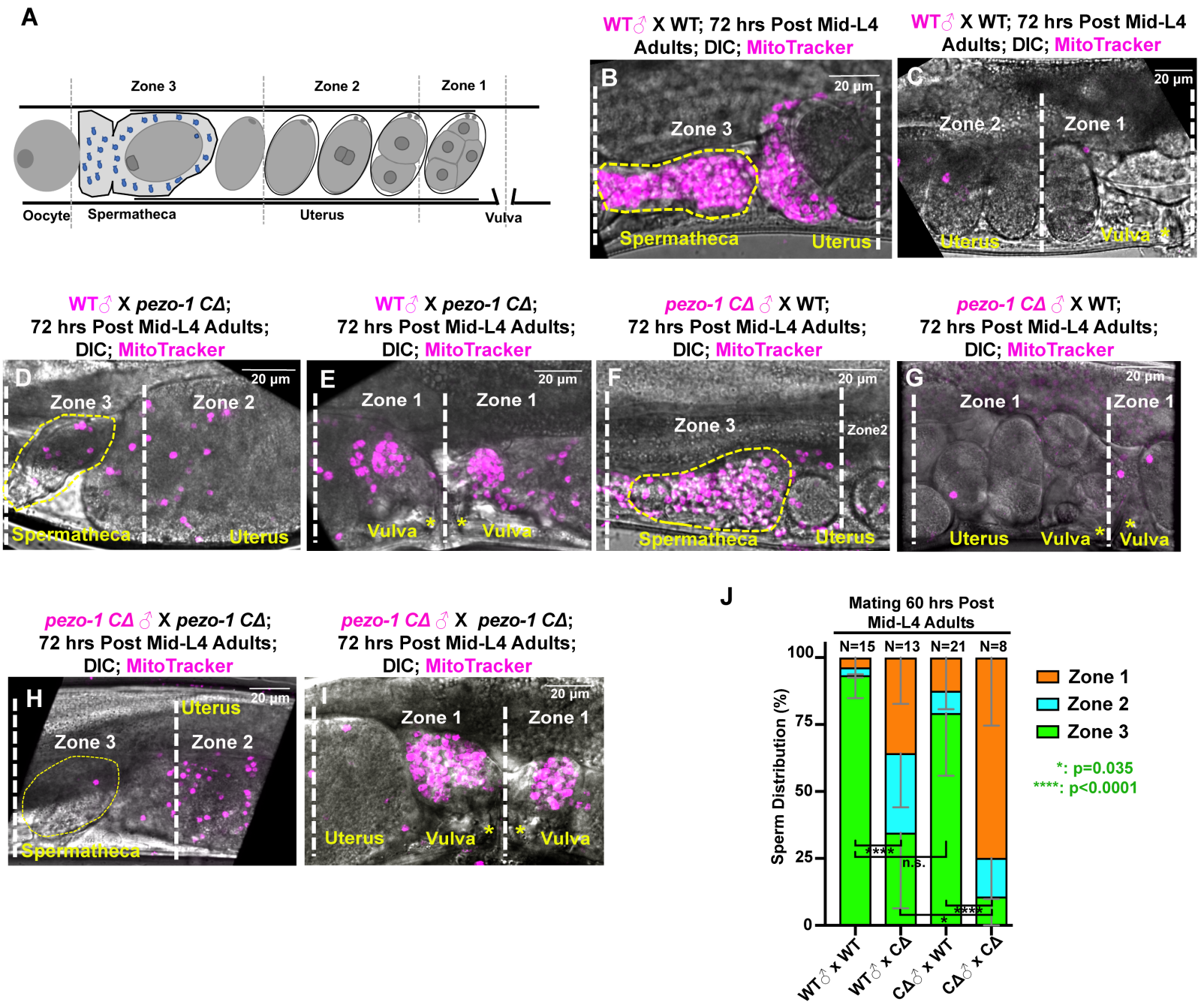
A
Zone 3
Zone 2
Zone 1
Oocyte
Spermatheca
Uterus
Vulva
WT♂ X WT; 72 hrs Post Mid-L4 Adults; DIC; MitoTracker
B
20 µm
Zone 3
Spermatheca
Uterus
WT♂ X WT; 72 hrs Post Mid-L4 Adults; DIC; MitoTracker
C
20 µm
Zone 2
Zone 1
Uterus
Vulva
WT♂ X pezo-1 CΔ; 72 hrs Post Mid-L4 Adults; DIC; MitoTracker
D
20 µm
Zone 3
Zone 2
Spermatheca
Uterus
WT♂ X pezo-1 CΔ; 72 hrs Post Mid-L4 Adults; DIC; MitoTracker
E
20 µm
Zone 1
Zone 1
Vulva
Vulva
pezo-1 CΔ ♂ X WT; 72 hrs Post Mid-L4 Adults; DIC; MitoTracker
F
20 µm
Zone 3
Zone2
Spermatheca
Uterus
pezo-1 CΔ ♂ X WT; 72 hrs Post Mid-L4 Adults; DIC; MitoTracker
G
20 µm
Zone 1
Zone 1
Uterus
Vulva
Vulva
pezo-1 CΔ ♂ X pezo-1 CΔ; 72 hrs Post Mid-L4 Adults; DIC; MitoTracker
H
20 µm
Uterus
Zone 3
Zone 2
Spermatheca
pezo-1 CΔ ♂ X pezo-1 CΔ; 72 hrs Post Mid-L4 Adults; DIC; MitoTracker
I
20 µm
Zone 1
Zone 1
Uterus
Vulva
Vulva
J
Mating 60 hrs Post Mid-L4 Adults
N=15
N=13
N=21
N=8
Sperm Distribution (%)
100
75
50
25
0
***
n.s.
*
****
WT♂ x WT
WT♂ x CΔ
CΔ♂ x WT
CΔ♂ x CΔ
Zone 1
Zone 2
Zone 3
*: p=0.035
****: p<0.0001

Figure 8

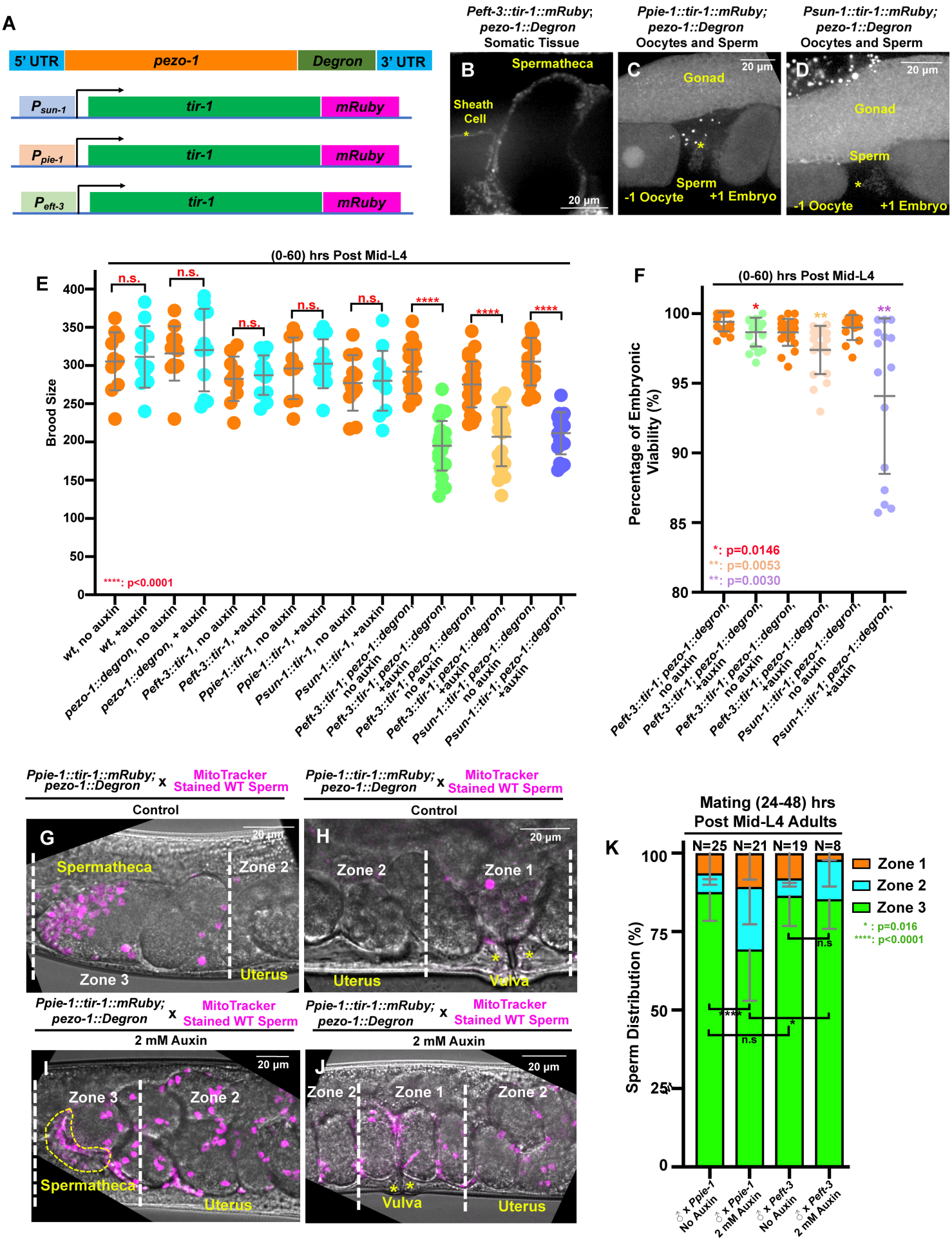
A
5' UTR
pezo-1
Degron
3' UTR
P sun-1
tir-1
mRuby
P pie-1
tir-1
mRuby
P eft-3
tir-1
mRuby
Peft-3::tir-1::mRuby; pezo-1::Degron Somatic Tissue
Ppie-1::tir-1::mRuby; pezo-1::Degron Oocytes and Sperm
Psun-1::tir-1::mRuby; pezo-1::Degron Oocytes and Sperm
B
Spermatheca
Sheath Cell
20 µm
C
Gonad
Sperm
-1 Oocyte
+1 Embryo
20 µm
D
Gonad
Sperm
-1 Oocyte
+1 Embryo
20 µm
E
(0-60) hrs Post Mid-L4
Brood Size
n.s.
****: p<0.0001
wt, no auxin
wt, +auxin
pezo-1::degron, no auxin
pezo-1::degron, + auxin
Peft-3::tir-1, no auxin
Peft-3::tir-1, +auxin
Ppie-1::tir-1, no auxin
Ppie-1::tir-1, +auxin
Psun-1::tir-1, no auxin
Psun-1::tir-1, +auxin
Peft-3::tir-1; pezo-1::degron, no auxin
Peft-3::tir-1; pezo-1::degron, +auxin
Peft-3::tir-1; pezo-1::degron, no auxin
Peft-3::tir-1; pezo-1::degron, +auxin
Psun-1::tir-1; pezo-1::degron, no auxin
Psun-1::tir-1; pezo-1::degron, +auxin
F
(0-60) hrs Post Mid-L4
Percentage of Embryonic Viability (%)
*: p=0.0146
**: p=0.0053
**: p=0.0030
Peft-3::tir-1; pezo-1::degron, no auxin
Peft-3::tir-1; pezo-1::degron, +auxin
Peft-3::tir-1; pezo-1::degron, no auxin
Peft-3::tir-1; pezo-1::degron, +auxin
Psun-1::tir-1; pezo-1::degron, no auxin
Psun-1::tir-1; pezo-1::degron, +auxin
Ppie-1::tir-1::mRuby; pezo-1::Degron x MitoTracker Stained WT Sperm
Control
G
Spermatheca
Zone 2
Zone 3
Uterus
20 µm
H
Zone 2
Zone 1
Uterus
Vulva
20 µm
2 mM Auxin
I
Zone 3
Zone 2
Spermatheca
Uterus
20 µm
J
Zone 2
Zone 1
Zone 2
Vulva
Uterus
20 µm
K
Mating (24-48) hrs Post Mid-L4 Adults
N=25
N=21
N=19
N=8
Zone 1
Zone 2
Zone 3
* : p=0.016
****: p<0.0001
n.s
Sperm Distribution (%)
♂ x Ppie-1 No Auxin
♂ x Ppie-1 2 mM Auxin
♂ x Peft-3 No Auxin
♂ x Peft-3 2 mM Auxin

Figure 8-figure supplement 1

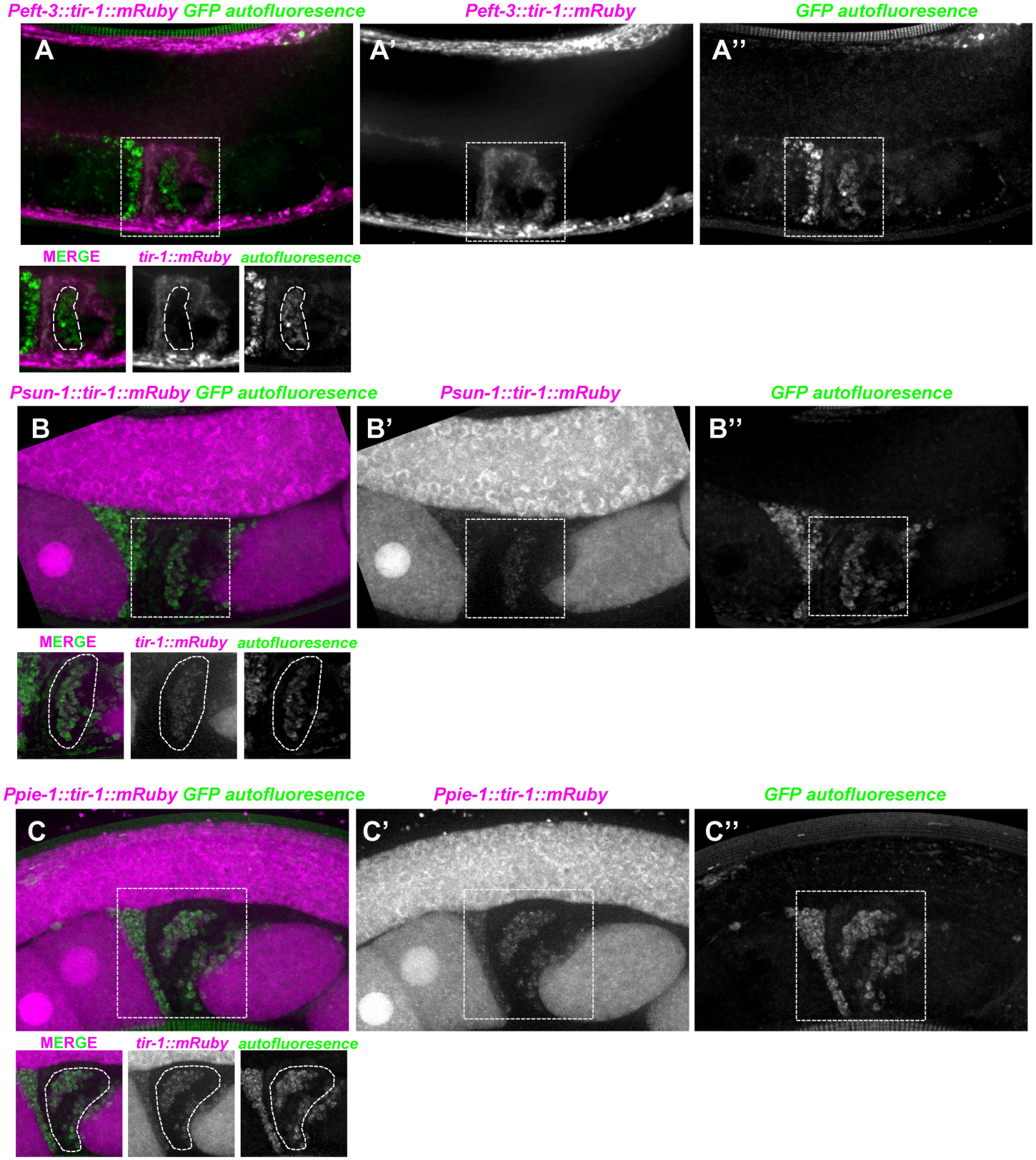

Figure 8-figure supplement 2

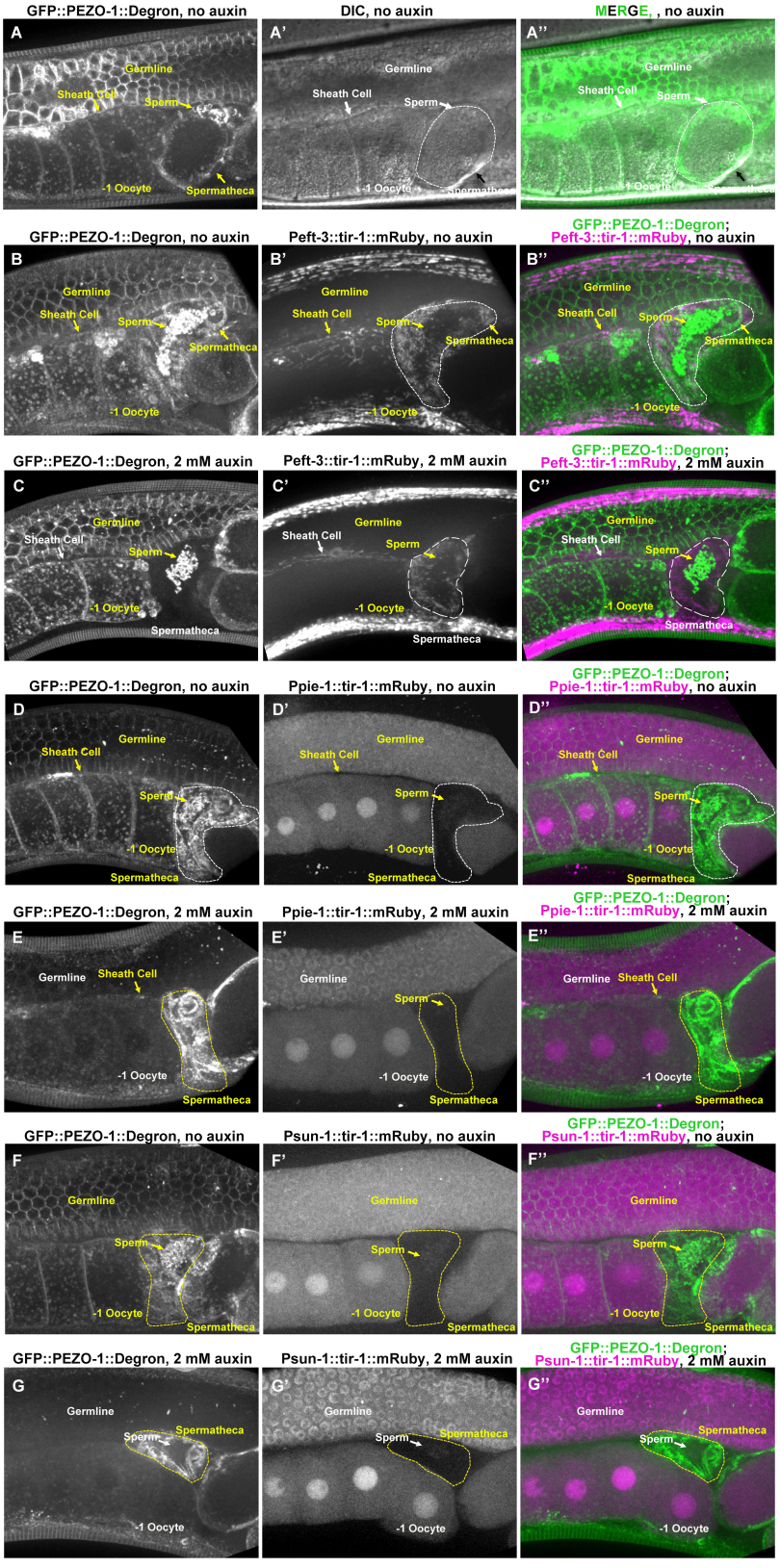

Figure 8- figure supplement 3

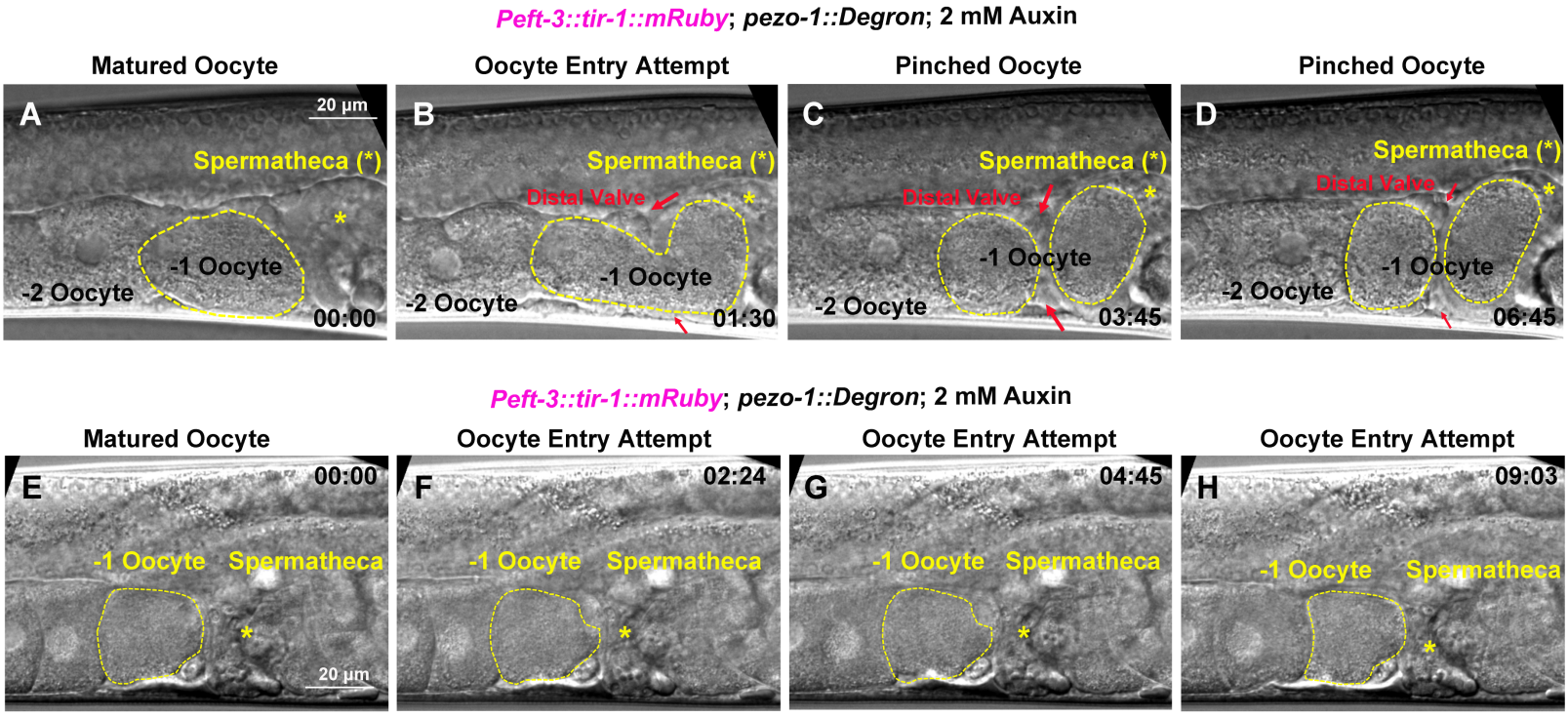

I

Genotype	Treatment	# Ovulations per hour	# Tested Gonad	# Pinched Oocyte	# Delayed Oocyte Entry
Peft-3::tir-1::mRuby; pezo-1::Degron	Control	1.71 ± 0.49	12	0% (0/13)	0% (0/13)
Peft-3::tir-1::mRuby; pezo-1::Degron	2 mM Auxin	1.14 ± 0.65	21	33.3% (9/27)	11.1% (3/27)

Figure 9

A

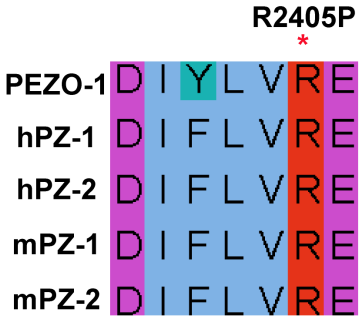

B

Genotype	# of hrs Post Mid-L4	Uteri with Ooplasmic Mass
pezo-1 (R2405P)	36 hours	100% (22/22)
	60 hours	100% (22/22)

C

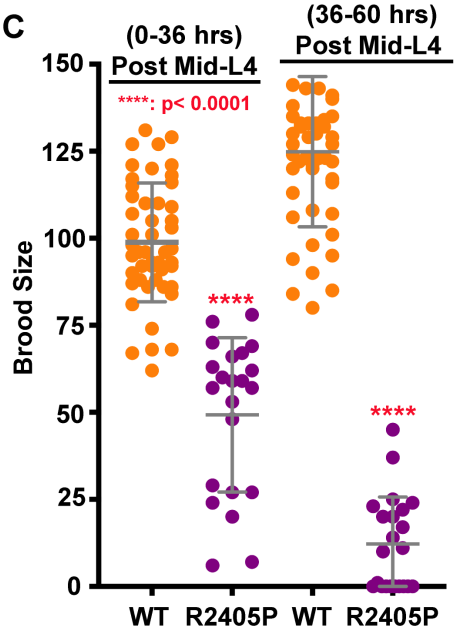

D

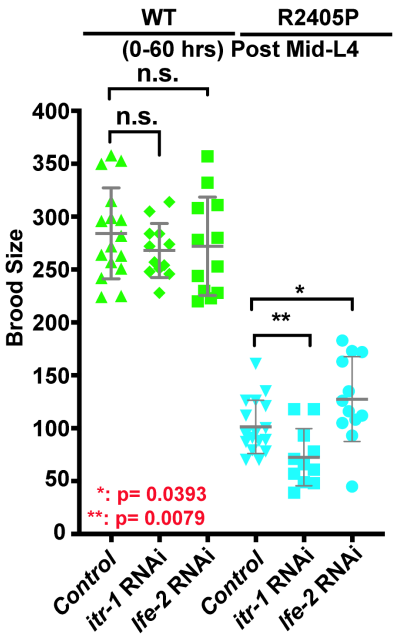

E

Genotype	# Hours Post Mid-L4	Male Genotype	# Ovulations per hour	# Tested Gonad Arms
pezo-1 (R2405P)	24 hours	N.A.	2.17 ± 1.34	12
pezo-1 (R2405P)	48 hours	N.A.	0.10 ± 0.32	10
pezo-1 (R2405P)	48 hours	*spe-9 (hc52ts); him-8*	1.53 ± 0.92	16

Figure 10

Step One: Sheath cell contraction, distal valve opening, ovulation and oocyte entry

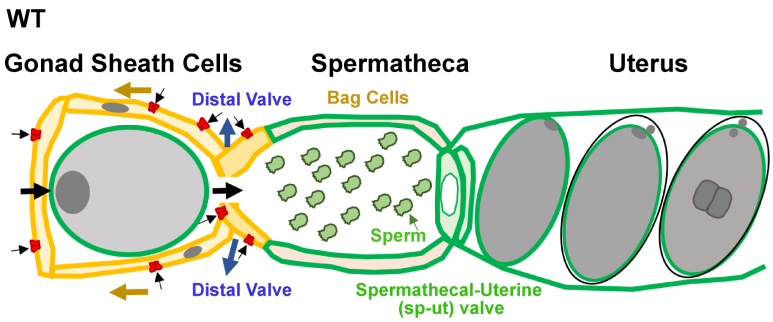

Step Two: Oocyte resides in the enclosed spermatheca until fertilization completes

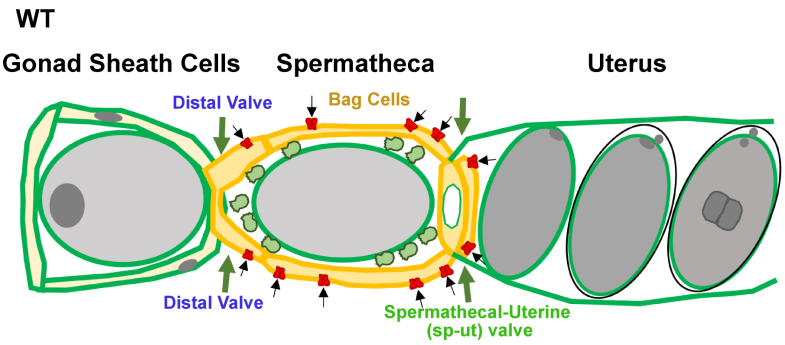

Step Three: Spermatheca dilates to allow fertilized oocyte to be expelled into the uterus